Preparation of biodegradable membrane utilizing chitosan and polyvinyl alcohol, and assessment of its performance after coating with graphene conductive ink

Meshram, Sumit Maya Moreshwar; Gonugunta, Prasad; Taheri, Peyman; Jourdin, Ludovic; Pande, Saket

DOI
10.3389/frmst.2025.1552368

Publication date
2025

Document Version
Final published version

Published in
Frontiers in Membrane Science and Technology

frontiers | Frontiers in Membrane Science and Technology

TYPE Original Research
PUBLISHED 06 August 2025
DOI 10.3389/frmst.2025.1552368

OPEN ACCESS

EDITED BY
Yucang Liang,
University of Tübingen, Germany

REVIEWED BY
Bharat Shrimant,
Dioxide Materials, United States
Aref Yarahmadi,
Department of Biology, Islamic Azad University, Iran

*CORRESPONDENCE
Sumit Maya Moreshwar Meshram,
S.M.Meshram@tudelft.nl

RECEIVED 27 December 2024
ACCEPTED 04 July 2025
PUBLISHED 06 August 2025

CITATION
Meshram SMM, Gonugunta P, Taheri P, Jourdin L and Pande S (2025) Preparation of biodegradable membrane utilizing chitosan and polyvinyl alcohol, and assessment of its performance after coating with graphene conductive ink.
Front. Membr. Sci. Technol. 4:1552368.
doi: 10.3389/frmst.2025.1552368

Preparation of biodegradable membrane utilizing chitosan and polyvinyl alcohol, and assessment of its performance after coating with graphene conductive ink

Sumit Maya Moreshwar Meshram[1]*, Prasad Gonugunta[2], Peyman Taheri[2], Ludovic Jourdin[3] and Saket Pande[1]

[1]Department of Water Management, Faculty of Civil Engineering and Geosciences, Delft University of Technology, Delft, Netherlands, [2]Department of Materials Science and Engineering (MSE), Faculty of Mechanical Engineering (ME), Delft University of Technology, Delft, Netherlands, [3]Department of Biotechnology, Faculty of Applied Sciences, Delft University of Technology, Delft, Netherlands

Biodegradable membranes are crucial for environmental applications, offering sustainable and low-impact solutions. These membranes play a vital role in biodegradable batteries by separating the anode and cathode while facilitating proton movement. The aim of this study is to develop a biodegradable membrane using biodegradable polymers such as chitosan (CS) and polyvinyl alcohol (PVA), reinforced with filter paper. In this research, a cost effective, biodegradable membranes using CS, PVA, and a 1:1 CS/PVA composite through solution-casting method were synthesized. The membranes were reinforced with cellulose filter paper and coated with water-resistant graphene conductive ink. Performance metrics, including swelling ratios, water uptake, ion exchange capacity, oxygen diffusion, proton conductivity, and degradation in compost tea, were evaluated. Uncoated CS membrane exhibited the highest water uptake (94.10%), while uncoated PVA membrane demonstrated the highest swelling ratio (150%) and ion exchange capacity (3.94 meq/g). Coated CS/PVA membrane showed the lowest oxygen diffusion coefficient (0.058×10^{-5} cm^2/s) and the highest proton conductivity (1.74 mS/cm). All membranes exhibited slow degradation over 100 days. The findings of this research have significant implications beyond the laboratory, presenting a biodegradable, cost-effective, and environmentally sustainable alternative to conventional membranes. These membranes can be utilized in the construction of biobatteries, which, in turn, can be employed to power low-cost devices.

KEYWORDS

membrane, biopolymer, chitosan, polyvinyl alcohol, graphene conductive ink

1 Introduction

For environmental applications, biodegradable membranes are crucial, as they offer an environmentally sustainable approach for addressing pollution, while conserving natural resources (Janakiraman et al., 2024). Applications include water electrolysis and wastewater treatment, gas separation, bioenergy, and biobatteries production (Ehsani et al., 2022; Osman et al., 2024). Biobatteries are part of the broader initiative to develop environmentally sustainable energy storage solutions, which are essential for supporting renewable energy

systems (Bertaglia et al., 2024). They represent a promising avenue in sustainable energy technology, utilizing biological processes to generate electrical energy (Fraiwan et al., 2016). These biobatteries harness the power of microorganisms or enzymes to convert organic matter into electricity through biochemical reactions (Gao et al., 2020). Biobattery consist of an anode, a cathode, an electrolyte, and a membrane (Hassanzadeh and Choi, 2015; Hassanzadeh and Langdon, 2023). Membranes serve to keep the positive and negative half-cells apart, preventing the mixing of electrochemically active ions. At the same time, they allow the necessary ionic conductivity for specific ions that are not electrochemically active, such as H^+(Fraiwan and Choi, 2014; Long Doan et al., 2015; Yogesh and Srivastava, 2022). Also, they are impermeable to fuel and oxidizing gases (Vilela et al., 2019). Proton exchange membranes (PEM) are specialized membranes that facilitate the passage of protons across their surfaces (Fraiwan and Choi, 2014). This proton transfer through the PEM, occurring between the anode and cathode, is essential for maintaining electroneutrality (Lee and Choi, 2015). Commercially available PEMs are costly and non-degradable (González-Pabón et al., 2019), because they are fabricated using nafion, sulfonated polybenzimidazole, polysulfone, and sulfonated poly (ether ketone) (Wang L. et al., 2019; Sharma et al., 2024). In addition, nafion exhibits poor durability and low power density, and upon disposal, it releases numerous perfluorinated compounds, including toxic perfluorocarboxylic acids and other environmentally persistent and bioaccumulative substances (Brito dos Santos et al., 2024). Due to these aforementioned limitations, these membranes are not suitable for biobattery construction (Sharma et al., 2024). Hence, there is a need of alternative membranes which can be suitable in the construction of such biobatteries.

Biopolymers can be utilized for membranes preparation in biobatteries, owing to their sustainability, environmental benefits, and functional properties (Galiano et al., 2018; Muhamaruesa and Isa, 2020; Joshi et al., 2024; Patra et al., 2024). These biopolymers also provide a low-cost alternative to traditional membranes, contributing to cost reduction, biodegradability, and high strength owing to their robust intramolecular and intermolecular hydrogen-bonding networks. These properties makes them as valuable materials for applications requiring durability and stability (Cox and Litwinski, 1979; Wang L. et al., 2019; Wang L. et al., 2023). Various biopolymers are available in market, such as Chitosan (CS), Polyvinyl Alcohol (PVA), Polylactic acid (PLA) etc., as described in (Ghanbarzadeh et al., 2013; Alday et al., 2020; Reddy et al., 2021), which can be employed for the preparation of membranes. CS is a naturally occurring polysaccharide in animal based biomass resources that has various advantages, such as an eco-friendly nature, flexibility for structural modification, high hydrophilicity, cost efficiency, improved chemical stability, and the ability to form a membrane (Mukoma et al., 2004; Dharmadhikari et al., 2018; Muhmed et al., 2020; Zhao et al., 2020; Sheth et al., 2024). CS based membrane has been fabricated by blending with nanocellulose (nanoscale fibers of cellulose) and also by combining two or more polymer layers, particularly with a solid support layer for dimensional stability (Zhao et al., 2020). For example, Song et al. (2024) has fabricated CS nanofiber paper membrane via a papermaking process to use in lithium-ion batteries, Yang et al. (2022) designed CS modified filter paper separator for aqueous zinc batteries, and Guo et al. (2023) used CS hydrogel polyelectrolyte-modified cotton pad as dendrite-inhibiting separators in aqueous zinc-ion batteries. Also, Tian et al. (2024) fabricated a multifunctional membrane from polydopamine-modified waste paper and hydrothermal carbonized CS, through simple vacuum filtration for separating oil-in-water emulsions and for *in situ* dye removal under controllable pH conditions.

PVA is a biodegradable and water-soluble synthetic polymer with reactive chemical functionalities (Halima, 2016). Through appropriate modifications, in the chemical features of the PVA, it can be used as membrane (Maiti et al., 2012; Surti et al., 2024). Raja et al. (2022) has developed a paper-based ceramic separator using a low-cost paper substrate functionalized by the wet-coating method using duo-polymer (CS and PVA) and ceramic barium titanate nanopowder. Ridwan et al. (2024) made conductive solid electrolyte membranes by mixing potassium hydroxide (KOH), PVA, and glycerol with the addition of nanocrystalline cellulose paper. Li et al. (2017) prepare the a membrane by mixing cotton pulp with nylon (polyamide fiber), vinylon (acetalized PVA fiber), and polypropylene fiber for zinc-silver battery. Wang et al. (2020) fabricated a PVA/lyocell dual-layer paper-based separator by dual-layer forming papermaking process for using in Zinc -air batteries.

However, the incorporation of the above biopolymers into cellulose paper, whether through impregnation or other methods, results in increased vulnerability to swelling, water absorption, and deterioration (Sahu and Gupta, 2022; Mohammed et al., 2023). This susceptibility is particularly pronounced when the paper is stored in highly humid environments or exposed to conditions of elevated moisture making it not suitable for biobattery construction. To address these issues, surface treatments such as sizing and coating are often employed to enhance the water resistance properties of cellulose paper. Modifying the wettability of the cellulose paper surface with sizing agents or by applying hydrophobic coatings a water barrier can be created to protect the paper from moisture damage (Rhim et al., 2006). Several significant studies have recently explored the use of hydrophobic coatings. These coatings have been crafted from lignin-based carbon nanospheres (Wen et al., 2024), ORMOCER®s, which are inorganic–organic polymers (Solberg et al., 2023), diblock copolymer PMMA-b-P (MA-FPOSS) (Pan et al., 2021), Photothiol-X Ligations (Bretel et al., 2018), emulsions made from carnauba wax and alcohol with Nano-TiO_2 particles (Wang et al., 2017), polyvinylidene fluoride (PVDF)/SiO_2 microspheres (Gao et al., 2017), polyhydroxybutyrate (PHB) particles mixed with nanofibrillated cellulose (NFC) and plant wax (Rastogi and Samyn, 2017), and catechol (adhesive) moieties (García et al., 2014). Coated paper can provide enhanced features by reducing the porosity and roughness and improve the moisture barrier properties. If a barrier coating layer is applied, the cellulose substrate becomes resistant to humidity changes and as well as to dimensional instability (Agate et al., 2018). However, only a limited number of studies have investigated the application of conductive hydrophobic coatings on cellulose paper. Coatings are often employed as a simple and cost-effective method to improve the properties of paper substrates used in membrane preparation. Some studies has coated membranes using conductive inks such as by Li et al. (2022), where they have utilized carbon-based conductive inks as coatings on membranes. Veerubhotla et al. (2017) have applied coatings on Whatman filter paper, which served not only as a support for electrode fabrication but also as a membrane in the biobattery. They employed commercially available eyeliner containing carbon nanoparticles and Fe_3O_4 as a conductive ink without any

binder for the preparation of the membrane. Jenkins et al. (2012) have used filter paper coated with conducting carbon ink in the biobattery setup. As can be seen that there are a few studies done in which membrane has been prepared using biopolymers impregnated with cellulose paper coated with conductive ink. The cellulose filter paper is utilized as reinforcement because it serves as a porous base for membranes, providing a structure that can be easily saturated and coated with casting solutions. The fibrous nature of filter paper results in a complex and uneven surface, which is beneficial for membrane applications. It improves lamination strength and membrane performance without causing the support to swell or dissolve. Additionally, the high crystallinity of filter paper ensures a stable and durable structure for reinforcement (Prambauer et al., 2015; Tran and Ulbricht, 2023). Also, the graphene conductive ink provides exceptional electrical conductivity, flexibility, and potential for environmentally sustainable formulations. In comparison to other coatings, it demonstrates superior adhesion, high printing resolution, and the ability to enhance conductivity (Saidina et al., 2019; Ashok Kumar et al., 2022).

While biodegradable polymers like CS and PVA have been widely studied, the integration of cellulose filter paper as a reinforcing scaffold for these membranes remains underexplored. Notably, the application of water-resistant graphene conductive ink as a coating on biodegradable polymer membranes has not been previously reported. Hence, in this study, eco-friendly and sustainable biodegradable membranes were synthesized from cellulose filter paper by impregnation with CS, PVA and 1:1 CS/PVA, followed by the coating with the mixture of graphene conductive ink and respective polymer CS, PVA and 1:1 CS/PVA. This study will help to create a membrane for biobatteries. they can power low-energy devices like soil moisture sensors. They can also be used in fuel cells that conduct protons, in water treatment to clean or remove salt, in eco-friendly packaging because they break down naturally, and in medical devices like temporary implants or systems that deliver drugs.

2 Experimental materials and methods

2.1 Materials and chemicals

All chemicals were analytically pure and used without further purification. Cellulose filter paper, with a 7.5 cm diameter and 200 μm thickness, and an average pore size of 1.5 μm, was purchased from Ahlstrom (Helsinki, Finland), Polyvinyl alcohol (molecular weight - 146,000–186,000, 99+% hydrolyzed), and Chitosan (high molecular weight) were purchased from Sigma-Aldrich. Conductive ink with graphene was purchased from FWG Limited, United Kingdom. PK booster compost tea was purchased from Biotabs (Netherlands).

2.2 Membrane synthesis

Membranes were prepared using the solution casting method. Initially, the polymers were dissolved in the solution, subsequently, the filter paper was immersed in it, and then dried in an oven at 60°C. Following this, the conductive ink was applied on the membrane using a paint brush. The detailed procedure is described in the subsequent subsections. Figure 1 illustrates the schematic of the membrane preparation method.

2.2.1 CS membrane

An aqueous solution of CS at a concentration of 2% (w/v) was prepared by dissolving 4 g of CS in 200 mL of acetic acid aqueous solution containing 2% (v/v). The mixture was stirred for 12 h at room temperature at 1000 rpm. To reduce the thickness of the solution, 150 mL of acetic acid was added to the previously prepared solution, and the mixture was stirred for one more hour. The solution was then filtered and stored at 4°C for 24 h. Subsequently, a 6 cm × 6 cm filter paper was immersed in the CS solution for 2 min to allow the CS solution to be absorbed by the filter paper, which was then left to dry at room temperature for 24 h. The filter paper was then dehydrated at 60°C for 6 h in an oven. The dry weight of the membrane was then measured to determine the amount of solution that had been absorbed by the filter paper.

The membrane was neutralized with 2 M NaOH for 5 min and washed with Milli-Q water. It was then crosslinked by immersion in 0.5 M H_2SO_4 for 24 h at room temperature. To remove excess cross-linking agent, the membrane was dipped in Milli-Q water and allowed to dry for 24 h at room temperature. The weights of the membranes were measured after cross-linking.

2.2.2 PVA membrane

PVA (10 g) was added to 100 mL of Milli-Q water (10% (w/v) aqueous PVA solution) and allowed to hydrate for 24 h. PVA was then dissolved by stirring at 500 rpm at 80°C for 2 h. The filter paper of size 6 cm × 6 cm, was then dipped in the PVA solution for 2 min, allowing the PVA solution to be absorbed by the filter paper. The filter paper was left to dry at room temperature for 24 h, and then at 60°C for another 6 h. The dry weight of the membranes was measured to determine the amount of solution absorbed by the filter paper.

The membranes were then treated with a 10% (v/v) solution of hydrogen peroxide for 1 h, washed, and crosslinked with a 10% (v/v) solution of sulfuric acid for 12 h. The weights of the membranes were measured after crosslinking.

2.2.3 CS/PVA membrane

Aqueous solutions of PVA and CS were mixed at a 1:1 (v/v) ratio (Ambili et al., 2019) and stirred for 2 h at 500 rpm. After mixing, the solution was stored at 4°C for 24 h. Filter paper, measuring 6 cm × 6 cm, was dipped in the CS/PVA solution for 2 min to allow the CS/PVA solution to be absorbed. The filter paper was left to dry at room temperature for 24 h and then dehydrated for 6 h in an oven at 60°C. The dry weights of the membranes were measured to determine the amount of solution absorbed by the filter paper.

The obtained membranes were neutralized with 2 M NaOH for 5 min and washed with Milli-Q water. Cross-linking was performed by immersing the membrane in 0.5 M H_2SO_4 for 24 h at room temperature, followed by dipping in Milli-Q water to remove excess cross-linking agent. The membranes were then allowed to dry at room temperature for 24 h. After crosslinking, the membrane weights were measured.

2.2.4 Graphene conductive ink solution

5 g of conductive graphene ink is mixed with 5 g of polymer solution of CS, PVA, and CS/PVA to prepare the conductive ink

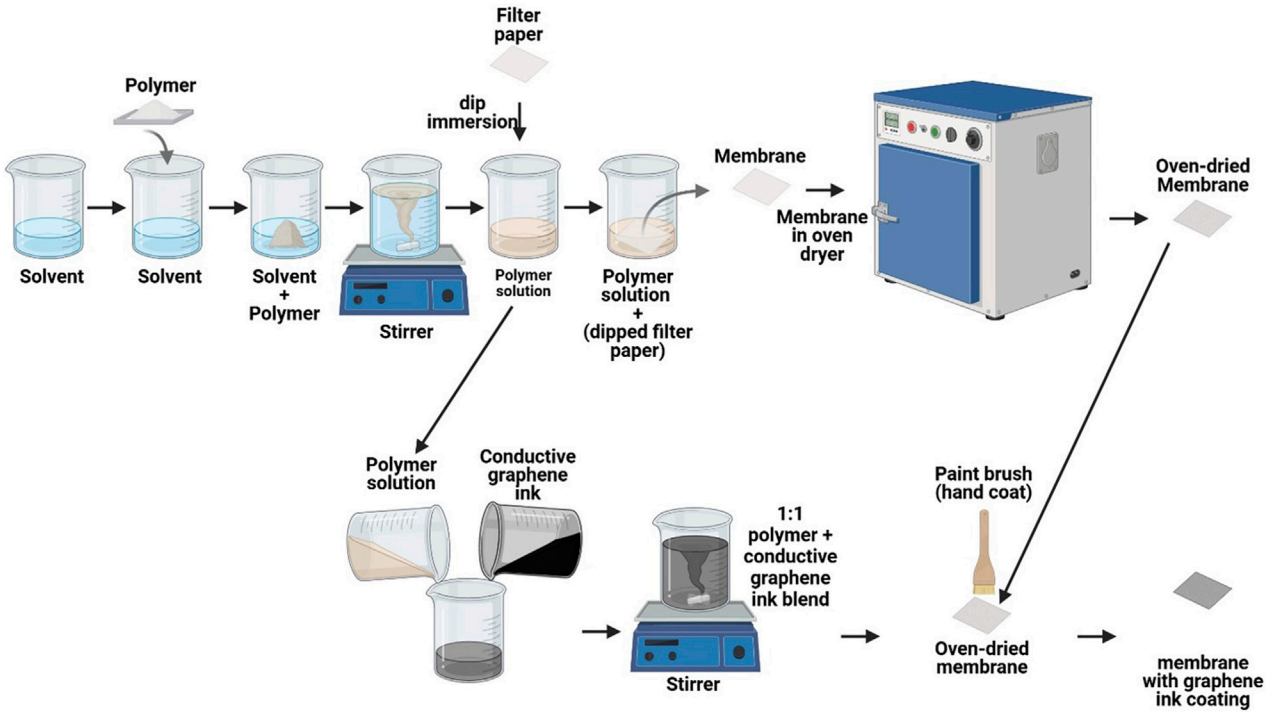

FIGURE 1
Schematic diagram of CS, PVA, and CS/PVA membranes prepared by solution casting method.

solution. The conductive ink solution mixture was stirred for 24 h at 200 rpm using a magnetic stirrer which results in 1:1 (Graphene ink: of CS, PVA, and CS/PVA) conductive ink solution. Subsequently, these 1:1 mixtures were coated on the polymer membranes using paint brush in two layers on one side of the membranes.

2.3 Membrane performance studies

2.3.1 Swelling ratio and water uptake capacity

2.3.1.1 Swelling ratio

The swelling ratios of the prepared membranes were calculated using the procedure described by González-Pabón et al. (2019) and the following equation:

$$\text{Swelling ratio } (\%) = \frac{T_{wet} - T_{dry}}{T_{dry}} \times 100 \quad (1)$$

where T_{wet} represents the thickness of the wet membranes obtained after soaking in Milli-Q water for 24 h and T_{dry} is the thickness of the respective dry membranes. The thickness of the membranes was measured using a digital vernier caliper (range: 0–150 mm; accuracy: 0.2 mm; resolution: 0.1 mm). Measurements were taken at various locations on the membranes, and the average thickness was subsequently calculated.

2.3.1.2 Water uptake capacity

The water uptake capacity was determined by measuring membrane weight changes during the hydration process (González-Pabón et al., 2019). The membranes were first dried in an oven at 30°C for 15 h, and then weighed (W_{dry}). After drying, the membranes were immersed in Milli-Q water for an initial period of 1 min, wiped with tissue paper, and immediately weighed (W_{wet}). The procedure was repeated for several times. Finally, the membranes were stored in Milli-Q water and maintained at room temperature for 24 h to avoid the warping of the membrane and use them for subsequent experiments. The water uptake (W%) was calculated using the following equation:

$$\text{Water uptake capacity } (\%) = \frac{W_{wet} - W_{dry}}{W_{dry}} \times 100 \quad (2)$$

where W_{wet} represents the weight of the wet membranes obtained after soaking in Milli-Q water and W_{dry} is the weight of the respective dry membrane.

2.3.2 Ion exchange capacity (IEC)

IEC is a measure of the number of ions that a material can exchange. IEC was calculated using an acid-base titration method according to the procedure described by González-Pabón et al. (2019). Circular membrane pieces (12.57 cm^2) were weighed and subsequently immersed in 1 M H_2SO_4 aqueous solution for 24 h to saturate the ion-exchange sites of the membrane with hydrogen ions (H^+). Subsequently, the membranes were thoroughly washed with Milli-Q water to eliminate any residual H_2SO_4 and retain only the H^+ ions bound to the ion exchange sites on the membrane. Then the obtained membranes were subsequently immersed in 50 mL of 1 M NaCl solution for 24 h. Throughout this time frame, the H^+ ions within the membrane were substituted with Na^+ (sodium ions) from the NaCl solution, thereby allowing H^+ ions to be released into the solution, and

making it acidic. The solution containing the released H^+ was then titrated with a 0.01 M NaOH basic solution using phenolphthalein as an indicator. Phenolphthalein indicator was prepared by adding 1 g of Phenolphthalein powder in 100 mL solution containing 50 mL of ethanol and 50 mL of Milli-Q water. This indicator is commonly employed to evaluate the electrochemical properties (Li et al., 2022). This colorless indicator underwent a change to pink upon titration as a result of the H^+ ions released from the membrane being neutralized by the OH^- ions from the NaOH solution. When the pH of the solution reaches 8.2 or above, a color change occurred, resulting in a pink solution. The IEC (meq/g) values of the dry membranes were calculated using the following equation.

$$IEC = \frac{V_{NaOH} \times S_{NaOH}}{W_{dry}} \quad (3)$$

where V_{NaOH} is the volume of NaOH spent during titration and W_{dry} is the dry weight of the membrane (g).

IEC specifies the number of ions that a membrane can exchange within a solution. A higher IEC signifies that the membrane can exchange a large quantity of ions.

2.3.3 Conductivity determination

Understanding the proton conductivity is essential for designing batteries that ensure efficient energy transfer for improved performance and higher energy efficiency. The mechanisms to describe proton transfer across the membranes (usually the main charge transporter) are related to the "Grotthuss mechanism," where protons flow from one proton carrier to another. In this case, the proton moves through proton carrier molecules with functional groups, such as $-NH_2$, $-NH_3^{+,}$ or $-SO_3H$, which dissociate H^+ and form hydrogen bonds. There is also a second mechanism called the "vehicle mechanism." In this mechanism, protons combine with water molecules to produce hydronium ions (e.g., H_3O^+, $H_5O_2^+$, and $H_9O_4^+$), which can migrate through a stream of water (González-Pabón et al., 2021).

Electrochemical impedance spectroscopy (EIS) measurements were carried out using 3 electrode system setup to obtain the specific conductivities of all the synthesized membranes (Panawong et al., 2022) and to determine the effect of the conductive ink coating on proton conduction compared to uncoated membranes. EIS experiments were performed using an Autolab PGSTAT302N potentiostat equipped with an FRA impedance module at open-circuit potential (Rezaei Niya and Hoorfar, 2013; Magar et al., 2021). The impedance of a material, which is a measure of its opposition to alternating current (AC), is composed of two components: resistance (real impedance) and reactance (imaginary impedance). Conductivity measurements were performed on both coated and non-coated membranes. The analysis was performed in the frequency range of 0.1 Hz and 10^5 Hz with an amplitude of 0.01 V at room temperature under 100% relative humidity (RH) by immersing the membranes in Milli-Q water before each measurement. Conductivity was calculated using the following equation:

$$\sigma\left(\frac{S}{cm}\right) = \frac{d}{R_s \times S} \quad (4)$$

where σ is the conductivity (S/cm), *d* is the electrode distance (cm), R_S is the resistance obtained from the impedance data (Ω), and *S* is the membrane area (cm^2) (Tabata et al., 2022).

2.3.4 Oxygen diffusivity determination

Oxygen diffusivity play a significant role in battery design because oxygen is an electron acceptor (Ucar et al., 2017). It is essential to avoid competition between the electron acceptor used in the battery and oxygen. The tests were performed in an H-type reactor. Oxygen concentrations were measured in the anode chamber using a dissolved oxygen (DO) probe (G1610, Greisinger, Germany) (precision ±0.2 mg/L). Prior to the measurement, the DO probe was inserted into the anode chamber containing water (250 mL) and was made airtight after purging with pure N_2 gas to remove dissolved oxygen from the anode chamber. The concentration of dissolved oxygen in the anodic chamber was periodically recorded to observe oxygen diffusivity from the cathode chamber to the anode chamber.

The oxygen mass transfer coefficient k_{O_2} (cm/s), which characterizes oxygen permeability, was calculated from the cathode to the anode chamber over time using the mass balance in Equation 5 (González-Pabón et al., 2019):

$$k_{O_2} = \frac{-V}{A \times T} \times \ln\left[\left(\frac{C_{O_2} - C}{C_{O_2}}\right)\right] \quad (5)$$

where V is the volume of the anode chamber (300 mL i.e 300 cm^3), A is the cross-sectional area of the membrane (12.57 cm^2), C_{O_2} is the saturation concentration of oxygen in the water (assumed to be 7.8 mg/L), and C is the concentration of oxygen in the anode chamber at time 'T (sec)' (mg/L).

The oxygen diffusion coefficient (D_0, cm^2/s) was calculated using the wet membrane thickness (T_{wet}) (González-Pabón et al., 2019):

$$D_0 = k_{O_2} \times T_{wet} \quad (6)$$

2.3.5 Linear sweep voltammetry (LSV) studies

The performance of the circular membranes (12.57 cm^2) was evaluated by polarization studies. The membrane was used as a separator in an H-type reactor, where the anodic and cathodic compartments were 300 mL each, respectively. Platinum electrode (1 cm × 1 cm) and carbon felt (1 cm × 2 cm) were used as anode and cathode, respectively. The anode compartment was filled with 300 mL of Milli-Q water, whereas the cathode compartment was filled with 150 mL of a phosphate buffered (0.1 M, pH 7) solution containing potassium ferricyanide (150 mL, 0.1 M), in order to avoid cathodic limitations. Linear sweep voltammetry (LSV) was performed in the potential range of 0–2 V at a scan rate of 1 mV/s using a Squidstat Potentiostat.

2.3.6 Degradation testing in compost tea

Biodegradation tests of membranes were performed in 100% composted tea. First, compost tea was prepared according to (Marín et al., 2013; Atreya et al., 2023), with a 1:3 (v:v) compost: water ratio in a 0.9 L PET flask. Non-aerated compost tea was used, in which the compost was suspended in Milli-Q water at the proportion indicated and stored at 20°C for seven days in the dark with periodic homogenization. After 7 days, the compost tea was filtered through a sieve and used for testing. In total 6 samples of size 2 cm × 1 cm were cut from the main membrane. They were then dried in an oven at 50°C for 1 h, and their initial weight was

measured (m_i), after which two samples were immersed in three bottles, each of 25 mL of compost tea, for the desired days under airtight conditions. After 5, 50, and 100 days, the samples were removed and dried at 50°C, and the final weight (m_f) of the membranes were measured. The degradation is calculated by finding out the percentage weight loss by the formula,

$$\text{Percentage weight loss}\,(\%) = \left[\frac{(m_i - m_f)}{m_i}\right] \times 100 \qquad (7)$$

where m_i is the initial weight and m_f is the weight remaining after immersing the membranes in the compost tea.

2.3.7 Characterization of membranes

The hydrophobicity/hydrophilicity of the prepared membranes was quantified by measuring the contact angle of a water droplet with an optical tensiometer (Theta Lite, TL100-TL101) by using the sessile drop method. The contact angle was measured immediately after putting water droplet on the membrane surface (t = 0). The water droplet was left undisturbed for 5 min on the CS membrane and 10 min for PVA and CS/PVA membranes before remeasuring the another contact angle. The surface morphology and microstructure characteristics of membranes were studied using a scanning electron microscope (SEM, JSM-IT800). The thermal stability of membranes was investigated using thermogravimetric analyzer (TGA, Netzsch STA 409 C/CD) instrument under argon (Ar) atmosphere, in the range of 25°C–600°C and heating rate was 20°C min^{-1}. The mechanical properties of the membranes were assessed using a Z010 material tester (Zwick, Ulm, Germany). Test specimens were excised from membranes that had been immersed in Milli-Q water for 7 days, with dimensions of 60 mm in length and 10 mm in width. Prior to testing, the specimens were dried using tissue paper. The tensile measurement were performed on strips with dimensions of 10 mm × 60 mm at room temperature with a crosshead speed of 2 mm/min. Subsequently, the mechanical properties (tensile strength, young's modulus, and elongation at break) were determined.

All experiments were performed in triplicate, and descriptive statistics were applied using Origin software to calculate the mean and standard deviation values.

3 Results and discussion

3.1 Swelling ratio and water uptake capacity

Figures 2A–C illustrate the water uptake capacity (%), swelling ratio (%) (based on thickness), swelling based on area (i.e., in-plane direction) of the CS, PVA, and CS/PVA membranes, wherein uncoated samples are represented as plain and ink coated samples as hatched. These values were calculated using Equations 1, 2 and has been shown in Table 1. The CS membrane exhibited the highest water uptake capacity (94.10%), followed by PVA (63.87%) and CS/PVA (54.44%) in uncoated samples. CS membrane exhibits significantly higher water absorption capacity than PVA membrane because of its distinctive structure and the presence of ionotropic cross-links. Whereas PVA membrane exhibits lower water absorption owing to its differing chemical structure and cross-linking behavior, which constrains its hydrophilicity relative to CS-based materials (Sangeetha et al., 2022). In addition, the absorption of water in PVA membrane is lower due to the formation of intramolecular hydrogen bonds between adjacent hydroxyl (OH) groups, which effectively reduces the number of water molecules that can be hydrated per OH group. While each OH group can attract water, PVAs retain only approximately 2–2.2 water molecules in aqueous solution (Satokawa and Shikata, 2008).

PVA membrane (150%) showed the highest swelling ratio compared with CS membrane (2%) and CS/PVA membrane (111.67%) in the uncoated samples. Interestingly, the swelling ratio of the CS uncoated membrane was found to be almost negligible in comparison to the other membranes. This phenomenon can be attributed to the cellulose filter paper in CS, which, when exposed, exhibits a robust network structure formed by extensive hydrogen bonding among cellulose fibers. This structure effectively prevents swelling despite significant water uptake. The cellulose filter paper fibers are clearly depicted in Supplementary Figure S2A. Also, the compact arrangement ensures mechanical integrity and stability, enabling the membrane to function efficiently without excessive expansion (Li et al., 2021). The data depicted in Figures 2A,B indicate that the ink coated membrane (hatched lines) exhibited a lower water uptake capacity [CS (59.62 %), PVA (59.06 %), and CS/PVA (17.08 %)], and a lower swelling ratio [CS (1.50 %), PVA (127.27 %), and CS/PVA (10 %)] compared to the uncoated samples (plain lines). This suggested that the ink coating impeded the ability of the samples to absorb water. The water uptake and swelling ratio are low in the coated membranes because graphene is hydrophobic and repels water (Sun et al., 2023), creating a physical barrier on the cellulose fibers. This makes it harder for water molecules to penetrate (Wang J. et al., 2019) and acts as a structural reinforcement for this study. As the ink dries, it forms a network of interconnected flakes that strengthen the paper matrix. This reinforcement helps the paper to resist the internal pressure caused by the absorbed water, thereby reducing swelling (Gambhir et al., 2015).

To assess the swelling of the membrane based on area (i.e., in the plane direction), a rectangular strip of membrane measuring 10 mm in width and 60 mm in length was excised from the membrane, and the rectangular area was calculated. The swelling of the membrane was observed to be negligible, potentially due to the cellulose paper, which restricts the membrane's swelling in both length and width directions (i.e., in-plane) (Lee et al., 2016). Cellulose fibers in filter paper exhibit anisotropic swelling behavior, with greater expansion in the thickness direction than in-plane. This structural arrangement of aligned and bonded fibers restricts the membrane's swelling in the in-plane direction (Bloch et al., 2024; Hubbe et al., 2024).

3.2 Ion exchange capacity (IEC)

Figure 3 illustrates the IEC of the uncoated (plain) and ink coated (hatched) CS, PVA, and CS/PVA membranes in terms of milliequivalents per gram (meq/g). The IEC values were calculated using Equation 3 and are shown in Table 1. In the bar graph, the x-axis represents the membrane, and the y-axis represents the IEC. The plot indicates that the uncoated PVA (3.94 meq/g) membrane has the highest IEC, followed by the CS (1.82 meq/g) and CS/PVA

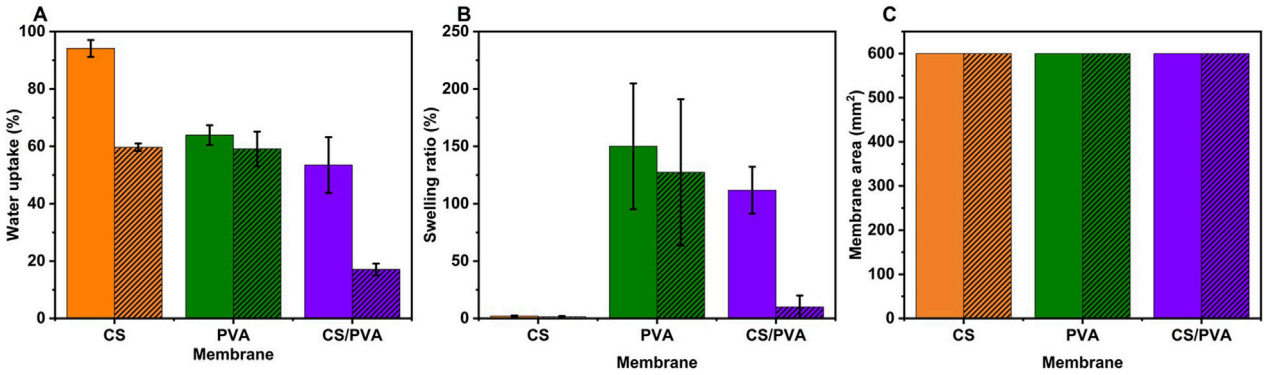

FIGURE 2
(A) Water uptake capacity, **(B)** Swelling ratio (based on thickness), and **(C)** Swelling area (in in-plane) of the membrane (plain graph -uncoated, hatched graph - ink coated).

TABLE 1 Average water uptake, swelling ratio, ion exchange capacity and proton conductivities of CS, PVA, and CS/PVA membranes.

Membrane	Water uptake (%)		Swelling ratio (%)		Ion exchange capacity (meq/g)		Proton conductivity (S/cm)	
	Uncoated	Coated	Uncoated	Coated	Uncoated	Coated	Uncoated	Coated
CS	94.10	59.62	2.00	1.50	1.82	0.61	7.8 μ	0.73 m
PVA	63.87	59.06	150.00	127.27	3.94	2.88	31.8 μ	1.51 m
CS/PVA	53.44	17.08	111.67	10.00	1.50	0.71	5.87 μ	1.74 m

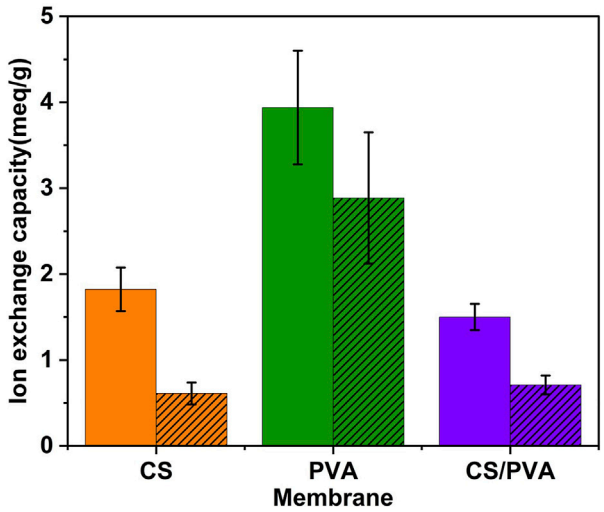

FIGURE 3
Ion exchange capacity of CS, PVA, and CS/PVA membranes (plain graph -uncoated samples, hatched graph - ink coated samples).

(1.50 meq/g) membranes. While for the coated membranes, IEC values decreased for all the three membranes: CS (0.61 meq/g), PVA (2.88 meq/g) and CS/PVA (0.71 meq/g). This could be because the ink coating acted as a barrier, preventing the ions from reaching the exchange sites on the membrane. The difference in performance between the coated and uncoated membranes was minimal for the PVA membranes. The IEC values in theory are approximately 3.1 for CS, around 11.6 for PVA, and about 7.36 meq/g for the CS/PVA.

Among the uncoated membranes, PVA exhibited the highest IEC at 3.94 meq/g, followed by CS at 1.82 meq/g, and the CS/PVA at 1.50 meq/g. The application of a graphene ink coating resulted in a reduction of IEC across all membrane types: CS decreased from 1.82 to 0.61 meq/g, for PVA from 3.94 to 2.88 meq/g, and for CS/PVA from 1.50 to 0.71 meq/g. This coating likely acted as a barrier, impeding ions from accessing the exchange sites on the membrane, potentially obstructing pores or functional groups involved in ion exchange. Other factors influencing IEC include the chemical structure, where PVA's configuration provides more ion exchange sites than CS, crosslinking, which can affect the availability of these sites, and hydrophilicity, as more hydrophilic materials generally exhibit higher IEC. Additionally, graphene's hydrophobic nature might reduce the water uptake necessary for ion transport. The smallest difference between coated and uncoated membranes was observed in PVA, suggesting its structure might still permit ion exchange despite the coating. Theoretical IEC values exceeded measured ones, indicating that not all potential exchange sites are accessible. Further experiments are necessary to gain a deeper understanding of the behaviour of these membranes. This could involve measuring IEC with different coating thicknesses, examining the membrane surface chemistry before and after coating, testing various coating materials to evaluate their effects, and investigating ion movement through coated membranes.

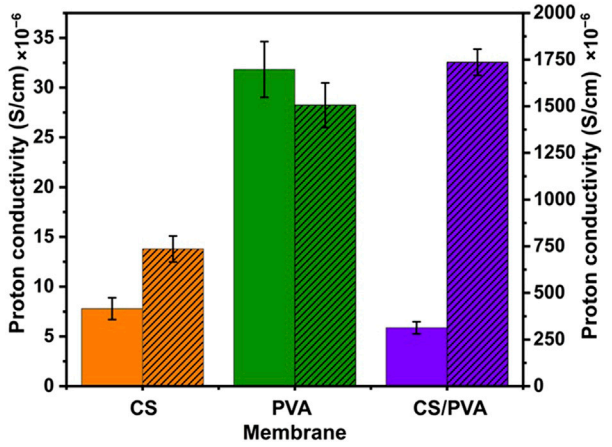

FIGURE 4
Proton conductivities attained for CS, PVA and CS/PVA membranes. Plain graph - uncoated (left y-axis), hatched graph - ink coated (right y-axis).

3.3 Conductivity determination

Supplementary Figures S3A, S3B shows the electrochemical impedance spectra of the CS, PVA, and CS/PVA membranes for both uncoated and ink coated membranes respectively. The real impedance, represented on the x-axis in ohms, and imaginary impedance, represented on the y-axis in ohms, are illustrated in Supplementary Figure S3. The EIS spectra indicated that the real impedances of all three membranes were higher at lower frequencies. This is because, at lower frequencies, the ions in the electrolyte have more time to diffuse into the membrane, which increases the resistance. At higher frequencies, the ions have less time to diffuse and the impedance decreases (Saghafi et al., 2023). The CS/PVA membrane exhibited the highest impedance among the uncoated membrane samples, whereas the CS membrane showed the highest impedance for the coated samples. The utilization of ink coating has a profound impact on the impedance of the membranes. Notably, the impedance of the coated membrane was lower than that of the uncoated membrane. This can be attributed to the fact that the graphene-based conductive ink applied to membranes improves the electrochemical properties, generates more interconnected channels for proton transfer, and facilitates efficient proton transfer across the membrane (Ahmed et al., 2023; Kushwaha et al., 2023; Muhmed et al., 2023).

The proton conductivities of the membranes were calculated using Equation 4 and are illustrated in Figure 4 and are reported in Table 1. The PVA membranes exhibited higher conductivities than the CS and CS/PVA membranes. These results are in agreement with the IEC data, where the highest IEC values were obtained with PVA membrane as the IEC and the proton conductivity was directly related (Wei et al., 2023). As reported in a previous study (Maiti et al., 2012), the proton permeability of the CS/PVA membrane was 11.2 mS/cm. However, in our study, the proton conductivity was found to be significantly lower 5.87 μS/cm when uncoated. This difference may be due to the cellulose filter paper used as reinforcement in the membranes, which may have impeded the proton flow. However, when coated, the conductivity increased to 1.74 mS/cm, even when cellulose filter paper was used as the reinforcement. This is in agreement with the study performed by Khan et al. (2015), where they have shown that the graphene enhances proton conductivity when blended with polymer. However, in case of PVA these values are 31.8 μS/cm in uncoated and 1.51 mS/cm in coated condition. The reduction in proton conductivity in the PVA membrane after coating with graphene can attributed to the high content of graphene nanofillers blocking ionic channels, which restricts the free movement of ions, thus hindering conductivity (Das et al., 2019). The IEC of a membrane depends on its material composition, structure, and surface treatments (Haldrup et al., 2016). CS membrane with abundant amine groups and hydrophilic properties, offers moderate proton exchange potential but has low density of exchangeable sites, resulting in reduced conductivity when uncoated (Palanisamy et al., 2023). When coated with ink containing acidic groups, the IEC improves, increasing conductivity. PVA forms flexible, water-retaining films but lacks strong acidic groups for high IEC. Its high conductivity indicates effective proton mobility, with coating providing slight enhancement. The CS/PVA membrane shows decreased conductivity when uncoated, likely due to phase separation (Aziz et al., 2017). However, coating significantly improves performance by introducing ion-exchange functionality and enhancing proton transport. The coating boosts IEC by adding proton-conducting groups and improving hydration, particularly in membranes with lower intrinsic ion exchange potential, demonstrating the importance of surface engineering for proton exchange applications.

3.4 Oxygen diffusivity measurement

The average oxygen concentration (mg/L) in the anode chamber, measured for 5 h, is shown in Figure 5A (uncoated) and Figure 5B (ink coated). These data are also given in Table 2, along with the oxygen diffusion, oxygen mass transfer coefficient, and oxygen diffusion coefficient which were calculated using Equation 5, 6, respectively. The average membrane thickness for the uncoated membranes is 0.01 cm for CS, 0.0183 cm for PVA, and 0.01 cm for CS/PVA. On the other hand, for the coated membranes, the thickness is 0.01 cm for CS, 0.025 cm for PVA, and 0.0125 cm for CS/PVA. The average oxygen concentration in the anode at the end of 5 h was the highest for PVA membrane (0.167 mg/L), whereas CS and CS/PVA membranes exhibited the same value of 0.100 mg/L when uncoated. However, in the coated membranes, these values were 0.100 mg/L, 0.067 mg/L, and 0.033 mg/L for CS, PVA, and CS/PVA, respectively. It can be seen that when the proton membranes are coated, the oxygen concentration in the anode chamber is less than that when uncoated because the graphene ink coating reduces oxygen diffusion (Topsakal et al., 2012). This is because the graphene coating creates a high-energy barrier that impedes the movement of oxygen atoms, making it difficult for them to penetrate through the membrane (Topsakal et al., 2012). The accuracy range of the oxygen diffusion probe was found to encompass the oxygen diffusion rates for all membranes, which was ±0.2 mg/L. Hence, no definitive conclusions could be drawn regarding the accuracy of the membranes based on data collected over a period of 5 h. To draw any meaningful conclusions regarding the accuracy of the membranes, it is necessary to conduct oxygen diffusion experiments over an

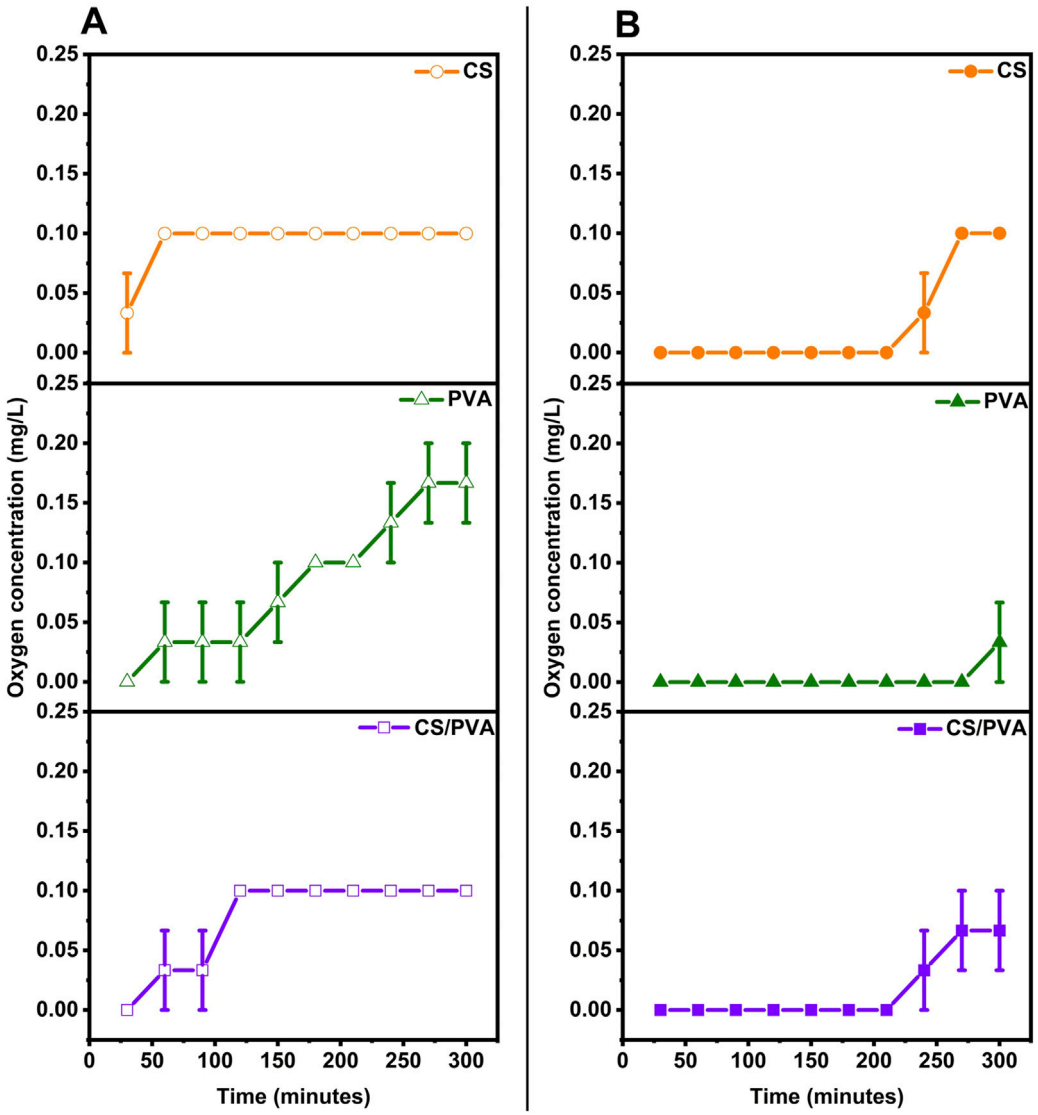

FIGURE 5
Average oxygen concentration (mg/L) of CS, PVA, and CS/PVA membranes. **(A)** uncoated, **(B)** ink coated.

TABLE 2 Oxygen diffusion, oxygen mass transfer coefficient and oxygen diffusion coefficient of CS, PVA, and CS/PVA membranes.

Membrane	Oxygen diffusion (avg at t = 5 h) (mg/L)		Oxygen mass transfer coefficient k_{O2} (cm/s) (10^{-5})		Oxygen diffusion coefficient D_o (cm^2/s) (10^{-5})	
	Uncoated	Coated	Uncoated	Coated	Uncoated	Coated
CS	0.100	0.100	1.425	1.425	0.142	0.142
PVA	0.167	0.067	2.391	0.953	0.437	0.238
CS/PVA	0.100	0.033	1.425	0.468	0.142	0.058

extended period of time or utilize an instrument that can measure significant variations in the oxygen diffusion rates more precisely.

When uncoated, PVA membrane has the highest value for the oxygen mass transfer coefficient, which is 2.391×10^{-5} cm/s followed by CS and CS/PVA membranes having the same value of 1.425×10^{-5} cm/s. Compared to the uncoated membranes, the coated membranes showed lower values for PVA (0.953×10^{-5} cm/s) and CS/PVA (0.468×10^{-5} cm/s), but for CS, it was the same as for uncoated membranes, which was 1.425×10^{-5} cm/s. The oxygen diffusion coefficient was the highest in PVA membrane (0.437×10^{-5} cm^2/s) under uncoated and coated conditions (0.238×10^{-5} cm^2/s). In general, the coating reduces the oxygen mass

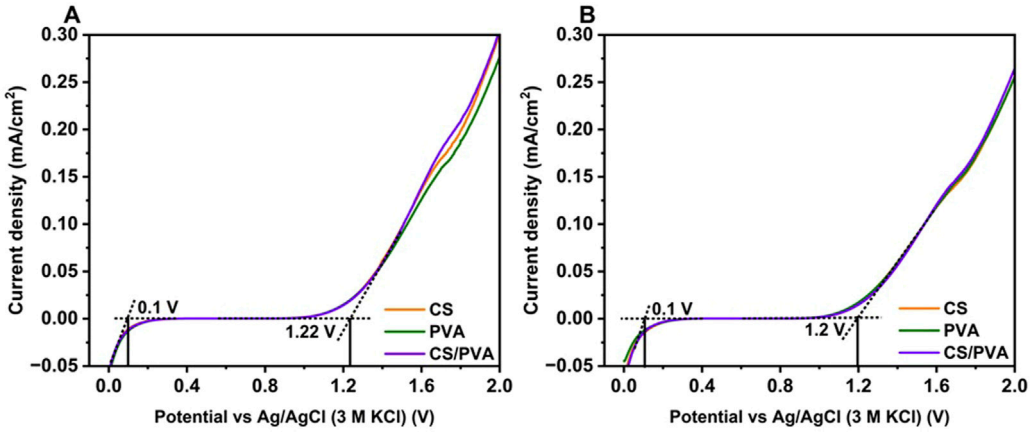

FIGURE 6
H-type reactor performance LSV curves of CS, PVA and CS/PVA membranes. **(A)** uncoated, **(B)** ink coated.

transfer and diffusion coefficients, with coated CS/PVA membrane demonstrating the lowest values.

It is noteworthy that although the viscosity of the polymer solutions (CS, PVA, and CS/PVA) likely affected the membrane coating and thickness (Zong et al., 2021), quantitative viscosity measurements were not conducted during membrane preparation. This constitutes a limitation of the present study, and future research will incorporate systematic viscosity characterization to more accurately correlate solution properties with membrane performance.

3.5 Linear sweep voltammetry (LSV)

The findings from the LSV curves, as illustrated in Figure 6A (uncoated) and Figure 6B (ink coated), reveal that there is a negligible current density between 0 and 1 V, indicating an electrochemical reaction in which no electrons are involved within this potential range for both the uncoated and coated membranes (i.e., CS, PVA, and CS/PVA). However, when the voltage was increased to more than 1 V, a considerable increase in the current flow was observed for the membranes, suggesting the onset of an electrochemical reaction. Previous studies have shown varied potential levels at which the current starts increasing, around the values reported here. For example, CS (1–1.3 V) (Shukur and Kadir, 2015), PVA (4.5 V) (Xiao et al., 2015), PVA - CS (1.70 V) (Kadir and Arof, 2011), CS - PVA and potassium hydroxide (KOH) (2 V) (Poosapati et al., 2021), CS with NH_4SCN and glycerol (2.09 V) (Aziz et al., 2021b), CS with DXN3 (1.54 V) (Aziz et al., 2021a), PVA–CS with NH_4I (1.33 V) (Shahab Marf et al., 2020), CS with NH_4NO_3 and ethylene carbonate (1.8 V) (Ng and Mohamad, 2008), and PVA with dextran and NH_4I (1.3 V) (Aziz et al., 2020) were noted. If the current remains stable below 1 V, without any sudden increase in current density, it can be considered as a positive indicator because it helps to minimize solvent evaporation and leakage within the electrochemical system. This is particularly beneficial for preventing any potential issues that may arise owing to solvent loss (Aziz et al., 2021a). For the uncoated and coated membranes, there was no variation in the current density between 0 and 1 V. For all the membranes (uncoated and coated), the current started rising after 1 V, hence it can be concluded that these membranes can be used in practical applications without undergoing any damage. These results suggest that the coating does not have a significant impact on the current density of the membranes, as there is only a slight decrease in the highest current density achieved by the coated membranes at a final potential of 2 V.

3.6 Degradation test

To create biodegradable batteries suitable for soil moisture sensors, it is essential that they have a functional lifespan of at least 100 days, as the typical growth period for crops ranges from 100 to 120 days (Wang et al., 2010). Given the significance of biodegradable membrane as a crucial component of batteries, it is vital to be aware of its degradation time. The study conducted on degradation of the membranes yielded degradation values, in terms of percentage of mass loss are listed in Table 3. These values were found out using Equation 7. It can be seen that the membranes degrade very slowly in 100 days at room temperature in compost tea (in between 2 wt% - 5 wt%), which is in agreement with the results shown in (Chiellini et al., 2003). Multiple factors may be responsible for the reduced degradation of these membranes, such as the polymer morphology, structure, chemical treatment, environmental conditions, and molecular weight (Chiellini et al., 2003; Samir et al., 2022). Previous studies have tested the degradation of CS, PVA, and CS/PVA membranes at various temperatures (Murmu et al., 2022; Vera et al., 2022) and have shown that degradation occurs beyond 250°C (Ambili et al., 2019; Vera et al., 2022). The degradation of CS occurs in the temperature range of 200°C–300°C and 500°C–600°C (Schaffer et al., 2018), and for PVA, it occurs at more than 50°C with a 99.9% degree of hydrolysis (Zhu and Ge , 2021). Based on these results, it can be inferred that the CS, PVA, and CS/PVA membranes exhibit stability at room temperature and in the presence of compost tea, membranes are not going under any degradation. Consequently, these membranes can be utilized for extended periods under normal environmental conditions without any degradation.

TABLE 3 Degradation of CS, PVA, and CS/PVA membranes in compost tea (100% concentration).

Time (days)	Membranes	CS			PVA			CS/PVA		
		m_i (avg)	m_f (avg)	% Mass loss	m_i (avg)	m_f (avg)	% Mass loss	m_i (avg)	m_f (avg)	% Mass loss
5	Coated	0.0255	0.0255	0.00	0.0545	0.0545	0.00	0.0295	0.0295	0.00
50		0.0265	0.0260	1.92	0.0565	0.0560	0.89	0.0280	0.0275	1.82
100		0.0255	0.0250	2.00	0.0555	0.0545	1.83	0.0290	0.0280	3.57
5	Uncoated	0.0240	0.0240	0.00	0.0510	0.0510	0.00	0.026	0.026	0.00
50		0.0265	0.0255	3.92	0.0510	0.0495	3.03	0.027	0.0265	1.89
100		0.0245	0.0235	4.26	0.0475	0.0450	5.56	0.026	0.025	4.00

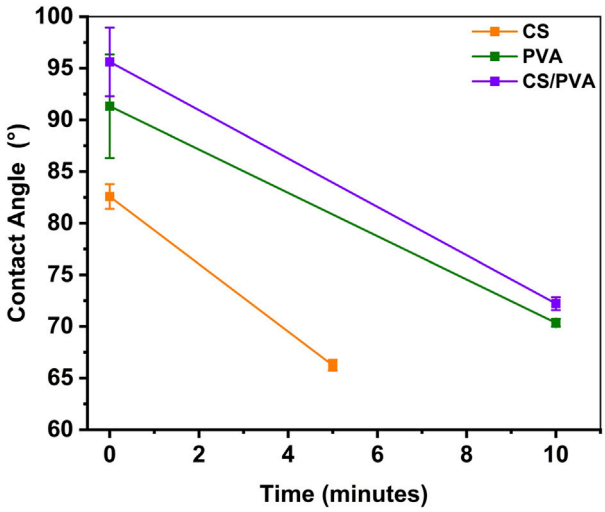

FIGURE 7
Mean contact angle vs. time for CS, PVA, and CS/PVA membranes.

3.7 Characterization

3.7.1 Contact angle

Contact angle measurements were conducted to determine whether the membranes exhibit hydrophobic or hydrophilic properties. Figure 7 shows the mean contact angle versus time of all the three membranes at beginning and after 5/10 min waiting time. Figure 8 shows photographs of contact angle measurements of all the three membranes. It was observed that the water droplet was gradually absorbed by the membranes, resulting in decreasing contact angles after waiting time. The absorption rate was found to be higher on CS membrane compared to on PVA and CS/PVA, membranes. The hydrophobicity of the membranes exhibited the following order for the membrane: CS/PVA > PVA > CS. The lower contact angle of CS membrane is attributed to the water uptake observation (Figure 2A), which illustrates that CS membrane exhibits a higher water uptake capacity compared to PVA and CS/PVA membranes. Study done by Tran et al. (2025) shows that the contact angle of the CS/PVA composite blended with graphene is significantly higher than the pure PVA, indicating the improved hydrophobicity in the composite films. Notably, the contact angle of all membranes decreased with time, regardless of the polymers used. Increasing the PVA percentage reduces the contact angle and hydrophilic characteristic of PVA in comparison to CS (Campa-Siqueiros et al., 2020).

3.7.2 SEM

Figure 9 presents the SEM images of CS, PVA, and CS/PVA membranes, each coated with a mixture of graphene ink and the corresponding polymer blend. The SEM images of CS membrane (Figures 9A1,A2) reveal that graphene flakes are readily observable. The graphene dispersed within the CS solution exhibits irregular wrinkled like structures. It can been that there are some uncovered areas, where cellulose of filter paper is exposed. Long Cellulose fibers are clearly visible in SEM images of CS shown in Supplementary Figure S2. The SEM images of PVA membrane demonstrate that a layer of graphene nanoparticles adheres to the surface of PVA molecules, where a smooth surface can be seen suggesting that the ink is uniformly distributed on the surface of the PVA membrane. The SEM images of CS/PVA membrane display a rough surface. Similar to CS membrane, there are some uncovered areas on CS/PVA membrane as seen in Figure 9C1, but smaller in area. Nano cellulose fibers are visible in both the CS and CS/PVA membranes as observed by Li et al. (209), Younas et al. (2019). To assess the coating thickness of the ink, SEM images were takes on the cross section of membranes. Upon examining the cross-section of the membranes, two distinct morphologies are evident: one associated with the ink and the other with the polymer. The absorption of ink into the CS membrane is observed to be non-uniform. This variation is attributed to the thickness of the graphene layer, where a thinner layer appears brighter and a thicker layer appears darker (Park et al., 2012). The thin layer of graphene ink exposes the underlying cellulose fiber, which is seen as brighter areas in the cross-section. In the case of PVA, the absence of bright areas indicates that the graphene ink blend is evenly distributed on the PVA membrane, forming a large dense layer (Eljaddi et al., 2021). In the CS/PVA membrane, two distinct, evenly distributed layers are visible, the upper darker layer is due to the graphene ink blend, while the lower brighter layer is attributed to the CS/PVA membrane. The absorption of the ink into the filter paper follows an increasing order: CS < CS/PVA < PVA. Analysis of the SEM images indicates

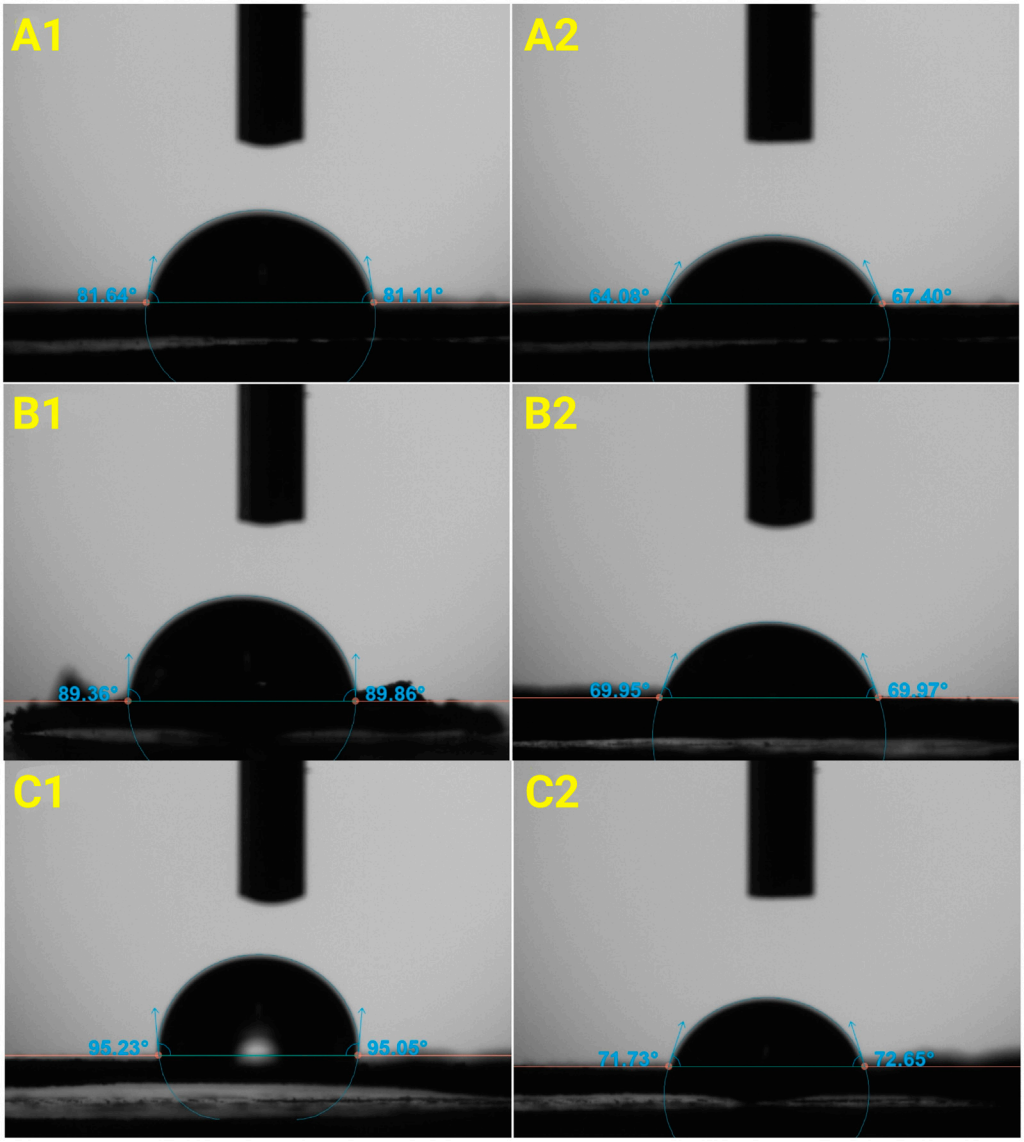

FIGURE 8
Mean contact angle measurements of CS, PVA, and CS/PVA membranes. **(A1)** (CS, t = 0 min), **(B1)** (PVA, t = 0 min), **(C1)** (CS/PVA, t = 0 min). **(A2)** (CS, t = 5 min), **(B2)** (PVA, t = 10 min), **(C2)** (CS/PVA, t = 10 min).

that a uniform ink coating layer cannot be achieved by manually applying the ink on the membranes. Therefore, it is necessary to employ the specialized coating technologies for applying graphene. Furthermore, observations of the PVA membranes reveal that the graphene ink is absorbed into the PVA. To prevent this absorption, an additional coating is required between the graphene ink and the PVA membrane, which will serve as a barrier to avoid ink absorption.

3.7.3 TGA

Figure 10 shows TGA curves of CS, PVA, and CS/PVA membranes coated with graphene ink. For CS, PVA, and CS/PVA the TGA curves showed that at about 100°C, the weight loss was about 1.5% which could be due to the loss of free water trapped in the CS, PVA, and CS/PVA molecules. A significant mass loss occurred at about 235°C, indicating the beginning of degradation, which was due to with the loss of amino and hydroxyl groups on CS membranes (Yang et al., 2018) and, due to the degradation of the main chain of the PVA polymers (Kandile and Nasr, 2023). At about 410°C, the weight loss was about 30% and the rate of degradation decreased due to the rigid and regular ring structure of CS (Yang et al., 2018). Generally, the temperatures where the biobatteries were used ranges from 4–90°C maximum. The examples of the reported temperature ranges of biobatteries are 4°C–25°C (Adekunle et al., 2019), 30°C–40°C (Mohammadifar and Choi, 2019), 65°C (Chen et al., 2016), and 90°C (Cheng et al., 2015). From the TGA curves, it can be seen that the three membranes investigated are stable below 100°C, hence these membranes can be used in the biobattery applications.

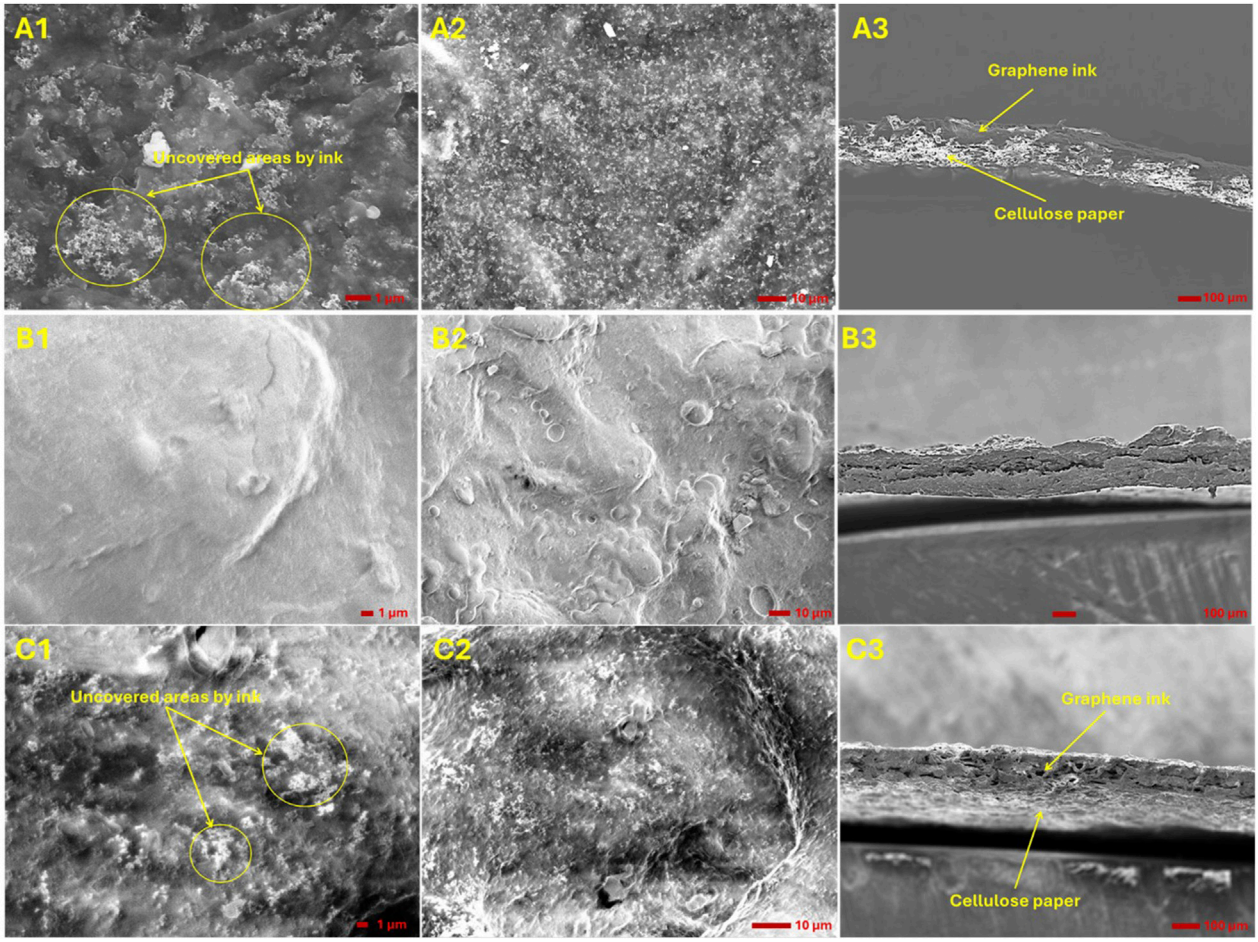

FIGURE 9
SEM images of CS, PVA, and CS/PVA membranes after coating with graphene ink. Panels **(A1, A2)**, **(B1, B2)**, and **(C1, C2)** depict the surface morphologies of the CS, PVA, and CS/PVA membranes, respectively, while panels **(A3-C3)** shows the cross-sectional morphologies of these membranes.

3.7.4 Mechanical properties

Figures 11A–D shows the Stress-strain curve, young"s" modulus, tensile strength, and elongation at break respectively which were extracted from the stress–strain curves of CS, PVA, and CS/PVA membranes, while the Supplementary Table S1 shows the exact calculated values from the test. The tensile measurements were performed on strips with dimensions of 10 mm × 60 mm at room temperature with a crosshead speed of 2 mm/min. The CS membrane exhibited a tensile strength of approximately 1.28 ± 0.29 MPa, a tensile strain of 6.48% ± 2.47%, and a Young's modulus of 0.38 ± 0.23 MPa. The PVA membrane demonstrated a tensile strength of about 0.58 ± 0.04 MPa, a tensile strain of 11.43% ± 1.14%, and a Young's modulus of 0.07 ± 0.01 MPa. The CS/PVA membrane, showed a tensile strength of approximately 3.73 ± 1.30 MPa, a tensile strain of 12.22% ± 0.29%, and a Young's modulus of 0.33 ± 0.08 MPa. The CS/PVA membrane showed the highest tensile strength values compared to CS and PVA membranes. The tensile strength of the CS, and PVA is lower which shows that it has higher flexibility and hence the CS and PVA membranes can be used in flexible biobattery design, as it was

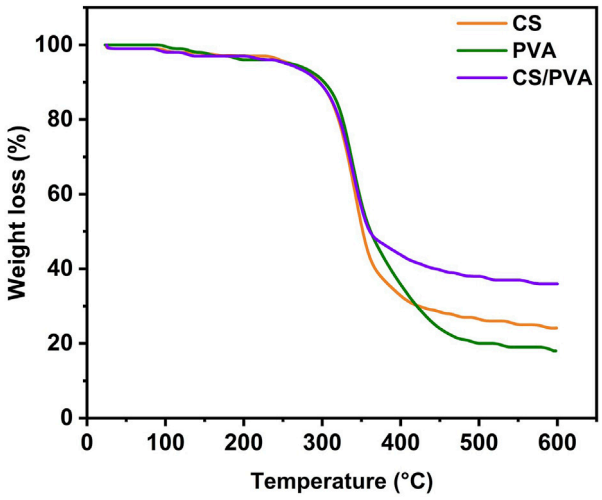

FIGURE 10
TGA analysis of CS, PVA, and CS/PVA membranes coated with graphene ink.

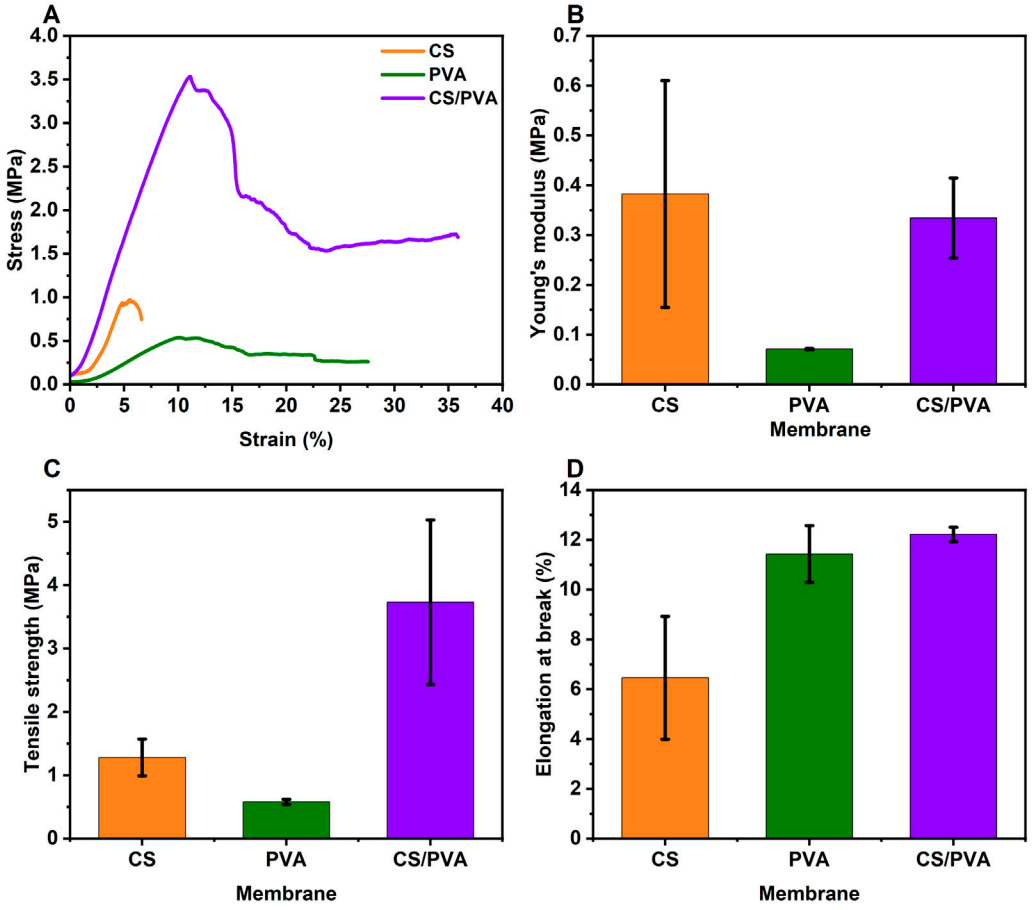

FIGURE 11
(A) Stress–strain curve, **(B)** Young's modulus plot, **(C)** tensile strength plot, and **(D)** elongation at break plot of CS, PVA, and CS/PVA membranes.

shown that the flexibility and tensile strength has a inverse relationship (Arpa et al., 2021). CS/PVA membrane showed the highest elongation at break values compared to CS and PVA membranes. Analysis of the data indicates that the selection of membranes should be tailored to the specific requirements of the applications. This is due to the absence of a consistent detectable trend in the various tensile strength, stress-strain, and elongation at break values.

4 Conclusion

This study illustrates the feasibility of fabricating biodegradable membranes utilizing CS, PVA, and CS/PVA composites reinforced with cellulose filter paper via the solution casting method. These membranes were subsequently coated with a water-resistant, conductive graphene ink to enhance their performance. The uncoated CS membrane exhibited the highest water uptake capacity at 94.10%, whereas the uncoated PVA membrane demonstrated the highest swelling ratio (150%) and ion exchange capacity (3.94 meq/g). Among all samples, the coated CS/PVA membrane exhibited the lowest oxygen diffusion coefficient (0.058×10^{-5} cm^2/s) and the highest proton conductivity (1.74 mS/cm). These findings suggest that the graphene-coated membranes possess superior electrochemical properties compared to their uncoated counterparts. All three membrane types exhibited slow degradation over 100 days at room temperature in compost tea, underscoring their potential for medium-term stability in water-rich environments. The integration of cellulose filter paper reinforcement and conductive graphene coating offers a promising strategy for the development of biobatteries and other biodegradable electronic devices. Characterization techniques such as scanning electron microscopy (SEM), thermogravimetric analysis (TGA), and contact angle measurements provided valuable insights into membrane morphology, thermal stability, and surface properties. Expanding the range of characterization tools could further enhance the understanding of membrane behaviour and performance. Future research should focus on optimizing membrane composition by exploring different CS/PVA ratios, alternative crosslinking methods, and modifications to improve specific properties such as proton conductivity and mechanical strength. The coating process could be refined to ensure more uniform graphene ink distribution, potentially through techniques such as spray coating, screen printing, or spin coating. Additionally, varying the properties of the cellulose filter paper (e.g., thickness, pore size) and incorporating additives could further tailor

membrane characteristics. Potential applications of these biodegradable membranes include biobatteries for low-power devices such as soil moisture sensors, fuel cells leveraging proton-conducting capabilities, water treatment utilizing selective permeability for purification or desalination, eco-friendly packaging due to their biodegradable nature, and biomedical devices, including temporary implants or drug delivery systems. Overall, this research opens promising avenues for the development of sustainable materials and energy technologies. Balancing key membrane properties such as water uptake, swelling, and conductivity will be essential for optimizing performance in targeted applications.

Data availability statement

The original contributions presented in this study are included within the article and in the Supplementary Material. For further inquiries, please contact the corresponding author.

Author contributions

SM: Conceptualization, Methodology, Visualization, Investigation, Funding acquisition, Data curation, and Writing - original draft. PG: Formal Analysis, Investigation, Data Curation, and Writing - review and editing. PT: Resources, Formal analysis, and Writing - review and editing. LJ: Conceptualization, Formal analysis, Methodology, Supervision, and Writing - review and editing. SP: Conceptualization, Methodology, Supervision, and Writing - review and editing.

Funding

The author(s) declare that financial support was received for the research and/or publication of this article. This work was supported by the Ministry of Social Justice and Special Assistance Department, Government of Maharashtra (India).

Acknowledgments

The authors extend their gratitude to Julia de Moraes Siedschlag and Patrick Teeuwisse for conducting the thermogravimetric analysis (TGA) and Raymond Dekker for mechanical testing on the membranes.

Conflict of interest

The authors declare that the research was conducted in the absence of any commercial or financial relationships that could be construed as a potential conflict of interest.

The author(s) declared that they were an editorial board member of Frontiers, at the time of submission. This had no impact on the peer review process and the final decision.

Generative AI statement

The author(s) declare that no Generative AI was used in the creation of this manuscript.

Publisher's note

Supplementary material

The Supplementary Material for this article can be found online at: https://www.frontiersin.org/articles/10.3389/frmst.2025.1552368/full#supplementary-material

References

Adekunle, A., Raghavan, V., and Tartakovsky, B. (2019). Real-time performance optimization and diagnostics during long-term operation of a solid anolyte microbial fuel cell biobattery. *Batteries* 5, 9. doi:10.3390/batteries5010009

Agate, S., Joyce, M., Lucia, L., and Pal, L. (2018). Cellulose and nanocellulose-based flexible-hybrid printed electronics and conductive composites – a review. *Carbohydr. Polym.* 198, 249–260. doi:10.1016/j.carbpol.2018.06.045

Ahmed, M. R., Mirihanage, W., Potluri, P., and Fernando, A. (2023). Highly stable graphene inks based on organic binary solvents. *Part. and Part. Syst. Charact.* 40, 2200153. doi:10.1002/ppsc.202200153

Alday, P. P., Barros, S. C., Alves, R., Esperança, J. M. S. S., Navarro-Segarra, M., Sabaté, N., et al. (2020). Biopolymer electrolyte membranes (BioPEMs) for sustainable primary redox batteries. *Adv. Sustain. Syst.* 4. doi:10.1002/adsu.201900110

Ambili, K., Joseph, S., and Sidharthan, A. (2019). A polyvinyl alcohol/chitosan blend proton exchange membrane for direct methanol fuel cell. *AIP Conf. Proc.* 2162, 020051. doi:10.1063/1.5130261

Arpa, M. D., Ünükür, M. Z., and Erim, Ü. C. (2021). Formulation, characterization and *in vitro* release studies of terbinafine hydrochloride loaded buccal films. *J. Res. Pharm.* 25(5), 659–673. doi:10.29228/jrp.58

Ashok Kumar, S. S., Bashir, S., Ramesh, K., and Ramesh, S. (2022). A comprehensive review: super hydrophobic graphene nanocomposite coatings for underwater and wet applications to enhance corrosion resistance. *FlatChem* 31, 100326. doi:10.1016/j.flatc.2021.100326

Atreya, M., Desousa, S., Kauzya, J.-B., Williams, E., Hayes, A., Dikshit, K., et al. (2023). A transient printed soil decomposition sensor based on a biopolymer composite conductor. *Adv. Sci.* 10, 2205785. doi:10.1002/advs.202205785

Aziz, S. B., Abdullah, O. G., Hussein, S. A., and Ahmed, H. M. (2017). Effect of PVA blending on structural and ion transport properties of CS:AgNt-Based polymer electrolyte membrane. *Polymers* 9, 622. doi:10.3390/polym9110622

Aziz, S. B., Brza, M. A., Hamsan, H. M., Kadir, M. F. Z., and Abdulwahid, R. T. (2021a). Electrochemical characteristics of solid state double-layer capacitor constructed from proton conducting chitosan-based polymer blend electrolytes. *Polym. Bull.* 78, 3149–3167. doi:10.1007/s00289-020-03278-1

Aziz, S. B., Brza, M. A., Hamsan, M. H., Kadir, M. F. Z., Muzakir, S. K., and Abdulwahid, R. T. (2020). Effect of ohmic-drop on electrochemical performance of EDLC fabricated from PVA:dextran:NH4I based polymer blend electrolytes. *J. Mater. Res. Technol.* 9, 3734–3745. doi:10.1016/j.jmrt.2020.01.110

Aziz, S. B., Nofal, M. M., Abdulwahid, R. T., Kadir, M. F. Z., Hadi, J. M., Hessien, M. M., et al. (2021b). Impedance, FTIR and transport properties of plasticized proton conducting biopolymer electrolyte based on chitosan for electrochemical device application. *Results Phys.* 29, 104770. doi:10.1016/j.rinp.2021.104770

Bertaglia, T., Costa, M., C., Lanceros-Méndez, S., and Crespilho, N. (2024). Eco-friendly, sustainable, and safe energy storage: a nature-inspired materials paradigm shift. *Mater. Adv.* 5, 7534–7547. doi:10.1039/D4MA00363B

Bloch, P.-Y., Bloch, J.-F., Olejnik, K., and Brissaud, D. (2024). Anisotropy and fiber orientation: a key player in the lateral imbibition of cellulose paper. *Fibers* 12, 56. doi:10.3390/fib12070056

Bretel, G., Rull-Barrull, J., Nongbe, M. C., Terrier, J.-P., Le Grognec, E., and Felpin, F.-X. (2018). Hydrophobic covalent patterns on cellulose paper through photothiol-X Ligations. *ACS Omega* 3, 9155–9159. doi:10.1021/acsomega.8b01317

Brito dos Santos, F., Kaschuk, J., Banvillet, G., Jalaee, A., Rojas, O. J., and Foster, E. J. (2024). Alternative proton exchange membrane based on a bicomponent anionic nanocellulose system. *Carbohydr. Polym.* 340, 122299. doi:10.1016/j.carbpol.2024.122299

Campa-Siqueiros, P., Madera-Santana, T. J., Ayala-Zavala, J. F., López-Cervantes, J., Castillo-Ortega, M. M., and Herrera-Franco, P. J. (2020). Nanofibers of gelatin and polivinyl-alcohol-chitosan for wound dressing application: fabrication and characterization. *Polímeros* 30, e2020006. doi:10.1590/0104-1428.07919

Chen, H., Zhu, Z., Huang, R., and Zhang, Y.-H. P. (2016). Coenzyme engineering of a hyperthermophilic 6-phosphogluconate dehydrogenase from NADP+ to NAD+ with its application to biobatteries. *Sci. Rep.* 6, 36311. doi:10.1038/srep36311

Cheng, K., Zhang, F., Sun, F., Chen, H., and Percival Zhang, Y.-H. (2015). Doubling power output of starch biobattery treated by the most thermostable isoamylase from an archaeon sulfolobus tokodaii. *Sci. Rep.* 5, 13184. doi:10.1038/srep13184

Chiellini, E., Corti, A., D'Antone, S., and Solaro, R. (2003). Biodegradation of poly (vinyl alcohol) based materials. *Prog. Polym. Sci.* 28, 963–1014. doi:10.1016/S0079-6700(02)00149-1

Cox, J. A., and Litwinski, G. R. (1979). Voltammetric ion selective electrode for the determination of nitrate. *Anal. Chem.* 51, 554–556. doi:10.1021/ac50040a024

Das, G., Kang, D., and Yoon, H. H. (2019). A proton conducting composite membrane based on polyvinyl alcohol and polyaniline-intercalated graphene oxide. *J. Korean Phys. Soc.* 74, 384–388. doi:10.3938/jkps.74.384

Dharmadhikari, S., Ghosh, P., and Ramachandran, M. (2018). Synthesis of proton exchange membranes for dual-chambered microbial fuel cells. *J. Serbian Chem. Soc.* 83, 611–623. doi:10.2298/jsc170902016d

Ehsani, M., Kalugin, D., Doan, H., Lohi, A., and Abdelrasoul, A. (2022). Bio-sourced and biodegradable membranes. *Appl. Sci.* 12, 12837. doi:10.3390/app122412837

Eljaddi, T., Giordano, L., and Roizard, D. (2021). Towards the synthesis of greener membranes: interest of PVA as porous support for membrane application in gas and liquid separations. *Sep. Purif. Technol.* 263, 118357. doi:10.1016/j.seppur.2021.118357

Fraiwan, A., and Choi, S. (2014). Bacteria-powered battery on paper. *Phys. Chem. Chem. Phys.* 16, 26288–26293. doi:10.1039/C4CP04804K

Fraiwan, A., Kwan, L., and Choi, S. (2016). A disposable power source in resource-limited environments: a paper-based biobattery generating electricity from wastewater. *Biosens. Bioelectron.* 85, 190–197. doi:10.1016/j.bios.2016.05.022

Galiano, F., Briceño, K., Marino, T., Molino, A., Christensen, K. V., and Figoli, A. (2018). Advances in biopolymer-based membrane preparation and applications. *J. Membr. Sci.* 564, 562–586. doi:10.1016/j.memsci.2018.07.059

Gambhir, S., Jalili, R., Officer, D. L., and Wallace, G. G. (2015). Chemically converted graphene: scalable chemistries to enable processing and fabrication. *NPG Asia Mater* 7, e186. doi:10.1038/am.2015.47

Gao, J., Huang, X., Xue, H., Tang, L., and Li, R. K. Y. (2017). Facile preparation of hybrid microspheres for super-hydrophobic coating and oil-water separation. *Chem. Eng. J.* 326, 443–453. doi:10.1016/j.cej.2017.05.175

Gao, Y., Cho, J. H., Ryu, J., and Choi, S. (2020). A scalable yarn-based biobattery for biochemical energy harvesting in smart textiles. *Nano Energy* 74, 104897. doi:10.1016/j.nanoen.2020.104897

García, B., Saiz-Poseu, J., Gras-Charles, R., Hernando, J., Alibés, R., Novio, F., et al. (2014). Mussel-inspired hydrophobic coatings for water-repellent textiles and oil removal. *ACS Appl. Mater. Interfaces* 6, 17616–17625. doi:10.1021/am503733d

Ghanbarzadeh, B., and Almasi, H. (2013). Biodegradable polymers. *Biodegradation - Life of Science* (InTech). doi:10.5772/56230

González-Pabón, M., Cardeña, R., Cortón, E., and Buitrón, G. (2021). Hydrogen production in two-chamber MEC using a low-cost and biodegradable poly(vinyl) alcohol/chitosan membrane. *Bioresour. Technol.* 319, 124168. doi:10.1016/j.biortech.2020.124168

González-Pabón, M. J., Figueredo, F., Martínez-Casillas, D. C., and Cortón, E. (2019). Characterization of a new composite membrane for point of need paper-based micro-scale microbial fuel cell analytical devices. *PLoS One* 14, e0222538. doi:10.1371/journal.pone.0222538

Guo, J., Wang, Y., Li, S., Qin, Y., Meng, Y., Jiang, L., et al. (2023). Chitosan hydrogel polyelectrolyte-modified cotton pad as dendrite-inhibiting separators for stable zinc anodes in aqueous zinc-ion batteries. *J. Power Sources* 580, 233392. doi:10.1016/j.jpowsour.2023.233392

Haldrup, S., Catalano, J., Hinge, M., Jensen, G. V., Pedersen, J. S., and Bentien, A. (2016). Tailoring membrane nanostructure and charge density for high electrokinetic energy conversion efficiency. *ACS Nano* 10, 2415–2423. doi:10.1021/acsnano.5b07229

Halima, N. B. (2016). Poly(vinyl alcohol): review of its promising applications and insights into biodegradation. *RSC Adv.* 6, 39823–39832. doi:10.1039/C6RA05742J

Hassanzadeh, N., and Langdon, T. G. (2023). Invited viewpoint: biodegradable Mg batteries. *J. Mater Sci.* 58, 13721–13743. doi:10.1007/s10853-023-08828-2

Hubbe, M. A., Sjöstrand, B., Lestelius, M., Håkansson, H., Swerin, A., and Henriksson, G. (2024). Swelling of cellulosic fibers in aqueous systems: a review of chemical and mechanistic factors. *BioResources* 19, 6859–6945. doi:10.15376/biores.19.3.hubbe

Janakiraman, V., Sowmya, S., and Thenmozhi, M. (2024). Biopolymer based membrane technology for environmental applications. *Phys. Sci. Rev.* 9, 2051–2076. doi:10.1515/psr-2022-0222

Jenkins, P., Tuurala, S., Vaari, A., Valkiainen, M., Smolander, M., and Leech, D. (2012). A comparison of glucose oxidase and aldose dehydrogenase as mediated anodes in printed glucose/oxygen enzymatic fuel cells using ABTS/laccase cathodes. *Bioelectrochemistry* 87, 172–177. doi:10.1016/j.bioelechem.2011.11.011

Joshi, J. S., Langwald, S. V., Ehrmann, A., and Sabantina, L. (2024). Algae-based biopolymers for batteries and biofuel applications in comparison with bacterial biopolymers—a review. *Polymers* 16, 610. doi:10.3390/polym16050610

Kadir, M. F. Z., and Arof, A. K. (2011). Application of PVA–chitosan blend polymer electrolyte membrane in electrical double layer capacitor. *Mater. Res. Innovations* 15, s217–s220. doi:10.1179/143307511X13031890749299

Khan, A., Asmatulu, R., and Hwang, G. (2015). Proton conductivity of graphene-based polymer electrolyte membrane. *ECS Trans.* 69, 569–577. doi:10.1149/06917.0569ecst

Kushwaha, A., Sharma, A., Bhatt, B. B., Mukhopadhyay, A., and Gupta, D. (2023). Inkjet-Printed graphene-modified aluminum current collector for high-voltage lithium-ion battery. *ACS Appl. Energy Mater.* 6, 4168–4178. doi:10.1021/acsaem.2c03870

Lee, H., and Choi, S. (2015). An origami paper-based bacteria-powered battery. *Nano Energy* 15, 549–557. doi:10.1016/j.nanoen.2015.05.019

Lee, M., Kim, S., Kim, H.-Y., and Mahadevan, L. (2016). Bending and buckling of wet paper. *Phys. Fluids* 28, 042101. doi:10.1063/1.4944659

Li, H.-L., Liu, W., and Chen, X.-F. (2017). "Preparation of separator paper used in zinc-silver battery,"*Chung-kuo Tsao Chih*, 36 (6). 1–6. doi:10.11980/j.issn.0254-508X.2017.06.001

Li, T.-T., Yan, M., Zhong, Y., Ren, H.-T., Lou, C.-W., Huang, S.-Y., et al. (2019). Processing and characterizations of rotary linear needleless electrospun polyvinyl alcohol(PVA)/Chitosan(CS)/Graphene(Gr) nanofibrous membranes. *J. Mater. Res. Technol.* 8, 5124–5132. doi:10.1016/j.jmrt.2019.08.035

Li, X., Guo, Y., Meng, J., Li, X., Li, M., and Gao, D. (2022). Self-Powered carbon ink/filter paper flexible humidity sensor based on moisture-induced voltage generation. *Langmuir* 38, 8232–8240. doi:10.1021/acs.langmuir.2c00566

Li, Z., Qiu, F., Yue, X., Tian, Q., Yang, D., and Zhang, T. (2021). Eco-friendly self-crosslinking cellulose membrane with high mechanical properties from renewable resources for oil/water emulsion separation. *J. Environ. Chem. Eng.* 9, 105857. doi:10.1016/j.jece.2021.105857

Long Doan, T. N., Hoang, A., and Chen, P. (2015). Recent development of polymer membranes as separators for all-vanadium redox flow batteries. *RSC Adv.* 5, 72805–72815. doi:10.1039/C5RA05914C

Magar, H. S., Hassan, R. Y. A., and Mulchandani, A. (2021). Electrochemical impedance spectroscopy (EIS): principles, construction, and biosensing applications. *Sensors (Basel)* 21, 6578. doi:10.3390/s21196578

Maiti, J., Kakati, N., Lee, S. H., Jee, S. H., Viswanathan, B., and Yoon, Y. S. (2012). Where do poly(vinyl alcohol) based membranes stand in relation to Nafion® for direct methanol fuel cell applications? *J. Power Sources* 216, 48–66. doi:10.1016/j.jpowsour.2012.05.057

Marín, F., Santos, M., Diánez, F., Carretero, F., Gea, F. J., Yau, J. A., et al. (2013). Characters of compost teas from different sources and their suppressive effect on fungal phytopathogens. *World J. Microbiol. Biotechnol.* 29, 1371–1382. doi:10.1007/s11274-013-1300-x

Mohammadifar, M., and Choi, S. (2019). A solid phase bacteria-powered biobattery for low-power, low-cost, internet of Disposable Things. *J. Power Sources* 429, 105–110. doi:10.1016/j.jpowsour.2019.05.009

Mohammed, M., Jawad, A. J. M., Mohammed, A. M., Oleiwi, J. K., Adam, T., Osman, A. F., et al. (2023). Challenges and advancement in water absorption of natural fiber-reinforced polymer composites. *Polym. Test.* 124, 108083. doi:10.1016/j.polymertesting.2023.108083

Muhamaruesa, N. H. M., and Isa, M. I. N. M. (2020). "Chapter 19 - biopolymer membranes for battery applications," in *Biopolymer membranes and films*. Editors

M. A. de Moraes, C. F. da Silva, and R. S. Vieira (Elsevier), 477–502. doi:10.1016/B978-0-12-818134-8.00019-5

Muhmed, S. A., Jaafar, J., Ahmad, S. N. A., Mohamed, M. H., Ismail, A. F., Ilbeygi, H., et al. (2023). Incorporating functionalized graphene oxide in green material-based membrane for proton exchange membrane fuel cell application. *J. Environ. Chem. Eng.* 11, 109547. doi:10.1016/j.jece.2023.109547

Muhmed, S. A., Nor, N. A. M., Jaafar, J., Ismail, A. F., Othman, M. H. D., Rahman, M. A., et al. (2020). Emerging chitosan and cellulose green materials for ion exchange membrane fuel cell: a review. *Energ. Ecol. Environ.* 5, 85–107. doi:10.1007/s40974-019-00127-4

Mukoma, P., Jooste, B. R., and Vosloo, H. C. M. (2004). Synthesis and characterization of cross-linked chitosan membranes for application as alternative proton exchange membrane materials in fuel cells. *J. Power Sources* 136, 16–23. doi:10.1016/j.jpowsour.2004.05.027

Murmu, R., Roy, D., Patra, S. C., Sutar, H., and Choudhary, B. (2022). Preparation and characterization of red mud modified chitosan-PVA composite membrane for direct methanol fuel cell. *J. Electrochem. Energy Convers. Storage* 20. doi:10.1115/1.4055693

Ng, L. S., and Mohamad, A. A. (2008). Effect of temperature on the performance of proton batteries based on chitosan–NH4NO3–EC membrane. *J. Membr. Sci.* 325, 653–657. doi:10.1016/j.memsci.2008.08.029

Osman, A. I., Chen, Z., Elgarahy, A. M., Farghali, M., Mohamed, I. M. A., Priya, A. k., et al. (2024). Membrane technology for energy saving: principles, techniques, applications, challenges, and prospects. *Adv. Energy Sustain. Res.* 5, 2400011. doi:10.1002/aesr.202400011

Palanisamy, G., Muhammed, A. P., Thangarasu, S., and Oh, T. H. (2023). Investigating the sulfonated chitosan/polyvinylidene fluoride-based proton exchange membrane with fSiO2 as filler in microbial fuel cells. *Membranes* 13, 758. doi:10.3390/membranes13090758

Pan, A., Shi, C., Jia, M., and He, L. (2021). Novel fluoroalkyl polyhedral oligomeric silsesquioxane (FPOSS) macromers for fabricating diblock copolymer as self-cleaning coatings. *Prog. Org. Coatings* 151, 106097. doi:10.1016/j.porgcoat.2020.106097

Panawong, C., Tasarin, S., Saejueng, P., and Budsombat, S. (2022). Composite proton conducting membranes from crosslinked poly(vinyl alcohol)/chitosan and silica particles containing poly(2-acrylamido-2-methyl-1-propansulfonic acid). *J. Appl. Polym. Sci.* 139. doi:10.1002/app.51989

Park, M.-H., Kim, T.-H., and Yang, C.-W. (2012). Thickness contrast of few-layered graphene in SEM. *Surf. Interface Analysis* 44, 1538–1541. doi:10.1002/sia.4995

Patra, N., Ramesh, P., Donthu, V., and Ahmad, A. (2024). Biopolymer-based composites for sustainable energy storage: recent developments and future outlook. *J. Mater. Sci. Mater. Eng.* 19, 34. doi:10.1186/s40712-024-00181-9

Poosapati, A., Negrete, K., Thorpe, M., Hutchison, J., Zupan, M., Lan, Y., et al. (2021). Safe and flexible chitosan-based polymer gel as an electrolyte for use in zinc-alkaline based chemistries. *J. Appl. Polym. Sci.* 138, 50813. doi:10.1002/app.50813

Prambauer, M., Paulik, C., and Burgstaller, C. (2015). The influence of paper type on the properties of structural paper – polypropylene composites. *Compos. Part A Appl. Sci. Manuf.* 74, 107–113. doi:10.1016/j.compositesa.2015.04.004

Raja, M. W., Basu, R. N., Pramanik, N. C., Das, P. S., and Das, M. (2022). Paperator: the paper-based ceramic separator for lithium-ion batteries and the process scale-up strategy. *ACS Appl. Energy Mater.* 5, 5841–5854. doi:10.1021/acsaem.2c00188

Rastogi, V. K., and Samyn, P. (2017). Synthesis of polyhydroxybutyrate particles with micro-to-nanosized structures and application as protective coating for packaging papers. *Nanomaterials* 7, 5. doi:10.3390/nano7010005

Reddy, M. S. B., Ponnamma, D., Choudhary, R., and Sadasivuni, K. K. (2021). A comparative review of natural and synthetic biopolymer composite scaffolds. *Polym. (Basel)* 13, 1105. doi:10.3390/polym13071105

Rezaei Niya, S. M., and Hoorfar, M. (2013). Study of proton exchange membrane fuel cells using electrochemical impedance spectroscopy technique – a review. *J. Power Sources* 240, 281–293. doi:10.1016/j.jpowsour.2013.04.011

Rhim, J.-W., Lee, J.-H., and Hong, S.-I. (2006). Water resistance and mechanical properties of biopolymer (alginate and soy protein) coated paperboards. *LWT - Food Sci. Technol.* 39, 806–813. doi:10.1016/j.lwt.2005.05.008

Ridwan, F., Febriyan, N., Husin, M. A., and Aulia, F. (2024). A study on the effect of cellulose nanocrystalline paper on PVA-KOH electrolyte membranes for increasing ionic conductivity. *Int. J. Energy Prod. Manag.* 9 (2 9), 113–120. doi:10.18280/ijepm.090206

Saghafi, M., Chinnathambi, S., and Lemay, S. G. (2023). High-frequency phenomena and electrochemical impedance spectroscopy at nanoelectrodes. *Curr. Opin. Colloid and Interface Sci.* 63, 101654. doi:10.1016/j.cocis.2022.101654

Sahu, P., and Gupta, M. (2022). Water absorption behavior of cellulosic fibres polymer composites: a review on its effects and remedies. *J. Industrial Text.* 51, 7480S–7512S. doi:10.1177/1528083720974424

Saidina, D. S., Eawwiboonthanakit, N., Mariatti, M., Fontana, S., and Hérold, C. (2019). Recent development of graphene-based ink and other conductive material-based inks for flexible electronics. *J. Electron. Mater.* 48, 3428–3450. doi:10.1007/s11664-019-07183-w

Samir, A., Ashour, F. H., Hakim, A. A. A., and Bassyouni, M. (2022). Recent advances in biodegradable polymers for sustainable applications. *npj Mater Degrad.* 6, 68–28. doi:10.1038/s41529-022-00277-7

Sangeetha, E., Narayanan, A., and Dhamodharan, R. (2022). Super water-absorbing hydrogel based on chitosan, itaconic acid and urea: preparation, characterization and reversible water absorption. *Polym. Bull.* 79, 3013–3030. doi:10.1007/s00289-021-03641-w

Satokawa, Y., and Shikata, T. (2008). Hydration structure and dynamic behavior of poly(vinyl alcohol)s in aqueous solution. *Macromolecules* 41, 2908–2913. doi:10.1021/ma702793t

Schaffer, J. V., Lupatini, K. N., Machado, B., Silva, E. S., Ferracin, R. J., and Alves, H. J. (2018). Parameters effect on proton conductivity to obtain chitosan membranes for use as electrolytes in PEMFC. *Int. J. Energy Res.* 42, 1381–1385. doi:10.1002/er.3933

Shahab Marf, A., Abdullah, M., R., and Aziz, B. (2020). Structural, morphological, electrical and electrochemical properties of PVA: CS-based proton-conducting polymer blend electrolytes. *Membranes* 10, 71. doi:10.3390/membranes10040071

Sharma, A., Đelević, L., and Herkendell, K. (2024). Next-generation proton-exchange membranes in microbial fuel cells: overcoming nafion's limitations. *Energy Technol.* 12. doi:10.1002/ente.202301346

Sheth, P., Patil, D., Kandasubramanian, B., and Mayilswamy, N. (2024). Advancements in chitosan membranes for promising secondary batteries. *Polym. Bull.* 81, 15319–15348. doi:10.1007/s00289-024-05448-x

Shukur, M. F., and Kadir, M. F. Z. (2015). Hydrogen ion conducting starch-chitosan blend based electrolyte for application in electrochemical devices. *Electrochimica Acta* 158, 152–165. doi:10.1016/j.electacta.2015.01.167

Solberg, A., Zehner, J., Somorowsky, F., Rose, K., Korpela, A., and Syverud, K. (2023). Material properties and water resistance of inorganic–organic polymer coated cellulose paper and nanopaper. *Cellulose* 30, 1205–1223. doi:10.1007/s10570-022-04925-8

Song, Y., Zhao, G., Zhang, S., Xie, C., Yang, R., and Li, X. (2024). Chitosan nanofiber paper used as separator for high performance and sustainable lithium-ion batteries. *Carbohydr. Polym.* 329, 121530. doi:10.1016/j.carbpol.2023.121530

Sun, Y., Zhang, X., Wang, C., Bai, X., Fan, L., Fan, J., et al. (2023). Effect of poly(3,4-ethylenedioxythiophene): poly(styrenesulfonate) on low-iridium catalyst layer for proton exchange membrane water electrolysis. *J. Power Sources* 586, 233678. doi:10.1016/j.jpowsour.2023.233678

Surti, P. V., Kailasa, S. K., and Mungray, A. K. (2024). Development of a novel composite polymer electrolyte membrane for application as a separator in a dual chamber microbial fuel cell. *Industrial Eng. Chem. Res.* 63, 5182–5194. doi:10.1021/acs.iecr.3c04280

Tabata, K., Nohara, T., Nakazaki, H., Makino, T., Saito, T., Arita, T., et al. (2022). Proton conductivity dependence on the surface polymer thickness of core–shell type nanoparticles in a proton exchange membrane. *Nanoscale Adv.* 4, 4714–4723. doi:10.1039/D2NA00450J

Tian, S., Liu, C., Hu, H., Zhao, H., Yao, A., Lan, J., et al. (2024). Construction of waste paper-chitosan-based membranes with pH-tunable surface charge for efficient separation of oil-in-water emulsion and dye. *ACS Sustain. Chem. Eng.* 12, 10854–10868. doi:10.1021/acssuschemeng.4c02540

Topsakal, M., Şahin, H., and Ciraci, S. (2012). Graphene coatings: an efficient protection from oxidation. *Phys. Rev. B* 85, 155445. doi:10.1103/PhysRevB.85.155445

Tran, D. H., and Ulbricht, M. (2023). Cellulose-cellulose composite membranes for ultrafiltration. *J. Membr. Sci.* 672, 121426. doi:10.1016/j.memsci.2023.121426

Tran, N. T., Nguyen, G. T., Le, T. M., and Huynh, A. T. N. (2025). Chitosan/graphene oxide/Ag nanocomposites loaded in polyvinyl alcohol films as biodegradable, UV-blocking, and antibacterial film for fruit packaging. *J. Appl. Polym. Sci.* 142, e56677. doi:10.1002/app.56677

Ucar, D., Zhang, Y., and Angelidaki, I. (2017). An overview of electron acceptors in microbial fuel cells. *Front. Microbiol.* 8, 643. doi:10.3389/fmicb.2017.00643

Veerubhotla, R., Das, D., and Pradhan, D. (2017). A flexible and disposable battery powered by bacteria using eyeliner coated paper electrodes. *Biosens. Bioelectron.* 94, 464–470. doi:10.1016/j.bios.2017.03.020

Vera, J., Mosquera-Vargas, E., and Diosa, J. E. (2022). Thermal, electrical and structural study of polymeric membranes based on poly(vinyl alcohol), chitosan and phosphoric acid. *Appl. Phys. A* 128, 377–5. doi:10.1007/s00339-022-05526-9

Vilela, C., Silvestre, A. J. D., Figueiredo, F. M. L., and Freire, C. S. R. (2019). Nanocellulose-based materials as components of polymer electrolyte fuel cells. *J. Mater. Chem. A* 7, 20045–20074. doi:10.1039/C9TA07466J

Wang, D.-C., Lei, S.-N., Zhong, S., Xiao, X., and Guo, Q.-H. (2023). Cellulose-based conductive materials for energy and sensing applications. *Polymers* 15, 4159. doi:10.3390/polym15204159

Wang, J., Liu, Y., Fan, Z., Wang, W., Wang, B., and Guo, Z. (2019a). Ink-based 3D printing technologies for graphene-based materials: a review. *Adv. Compos Hybrid. Mater* 2, 1–33. doi:10.1007/s42114-018-0067-9

Wang, L., Zuo, X., Raut, A., Isseroff, R., Xue, Y., Zhou, Y., et al. (2019b). Operation of proton exchange membrane (PEM) fuel cells using natural cellulose fiber membranes. *Sustain. Energy Fuels* 3, 2725–2732. doi:10.1039/C9SE00381A

Wang, Y., He, B., and Zhao, L. (2017). Fabrication of hydrophobic coating on filter paper from self-emulsifying carnauba wax-alcohol emulsions with nano-TiO2 particles for water/diesel separation. *BioResources* 12, 7774–7783. doi:10.15376/biores.12.4.7774-7783

Wang, Y., Long, J., Hu, J., Sun, Z., and Meng, L. (2020). Polyvinyl alcohol/Lyocell dual-layer paper-based separator for primary zinc-air batteries. *J. Power Sources* 453, 227853. doi:10.1016/j.jpowsour.2020.227853

Wang, yu-min, Seydou, T., and Kerh, T. (2010). Applying evapotranspiration reference model and RainfallContribution index for agricultural water management plan in Burkina Faso. *Afr. J. Agric. Res.* 4, 1493–1504.

Wei, P., Sui, Y., Meng, X., and Zhou, Q. (2023). The advances development of proton exchange membrane with high proton conductivity and balanced stability in fuel cells. *J. Appl. Polym. Sci.* 140, e53919. doi:10.1002/app.53919

Wen, M., Wang, H., Ma, B., and Xiong, F. (2024). Photothermal performance of lignin-based nanospheres and their applications in water surface actuators. *Polymers* 16, 927. doi:10.3390/polym16070927

Xiao, W., Zhao, L., Gong, Y., Liu, J., and Yan, C. (2015). Preparation and performance of poly(vinyl alcohol) porous separator for lithium-ion batteries. *J. Membr. Sci.* 487, 221–228. doi:10.1016/j.memsci.2015.04.004

Yang, S., Liu, Y., Jiang, Z., Gu, J., and Zhang, D. (2018). Thermal and mechanical performance of electrospun chitosan/poly(vinyl alcohol) nanofibers with graphene oxide. *Adv. Compos Hybrid. Mater* 1, 722–730. doi:10.1007/s42114-018-0060-3

Yang, X., Wu, W., Liu, Y., Lin, Z., and Sun, X. (2022). Chitosan modified filter paper separators with specific ion adsorption to inhibit side reactions and induce uniform Zn deposition for aqueous Zn batteries. *Chem. Eng. J.* 450, 137902. doi:10.1016/j.cej.2022.137902

Yogesh, R., and Srivastava, N. (2022). "A detailed insight towards the role of microbial fuel cells for pharmaceutical wastewater treatment," in *Microbial fuel cell: electricity generation and environmental remediation*, 157–191.

Younas, M., Maryam, A., Khan, M., Nawaz, A. A., Jaffery, S. H. I., Anwar, M. N., et al. (2019). Parametric analysis of wax printing technique for fabricating microfluidic paper-based analytic devices (μPAD) for milk adulteration analysis. *Microfluid Nanofluid* 23, 38–10. doi:10.1007/s10404-019-2208-z

Zhao, G., Chen, Y., Li, X.-F., Zhang, S., and Situ, Y. (2020). Fabrication of highly proton-conductive chitosan whole-bio-membrane materials functionalized with adenine and adenosine monophosphate. *Green Chem.* 22, 2426–2433. doi:10.1039/c9gc04104d

Zhu, G., and Ge, M. (2021). Study on efficient degradation of polyvinyl alcohol in aqueous solution. *Environmental Challenges* 4, 100176. doi:10.1016/j.envc.2021.100176

Zong, C., Yang, X., Chen, D., Chen, Y., Zhou, H., and Jin, W. (2021). Rational tuning of the viscosity of membrane solution for the preparation of sub-micron thick PDMS composite membrane for pervaporation of ethanol-water solution. *Sep. Purif. Technol.* 255, 117729. doi:10.1016/j.seppur.2020.117729